



*PhD thesis*

Biomedical applications of inorganic nanoparticles:  
Magnetic Resonance Imaging and Hyperthermia

**Jesus Penaranda Avila**

Submitted for the degree of Doctor of Philosophy  
at the University of Milano-Bicocca

School of Doctorate in Nanotechnologies and Nanostructures  
XXVII Course  
University of Milano-Bicocca  
2015

Supervisor: Dr. Davide Prosperì



## List of abbreviations

AC	Alternating current
AMF	Alternating magnetic field
B	Magnetic induction
BBB	Blood-brain barrier
bp	Boiling point
BSA	Bovine serum albumin
CH <sub>3</sub> COOH	Acetic acid
CHCl <sub>3</sub>	Chloroform
CLIO	Crosslinked iron oxide
CoFe <sub>2</sub> O <sub>4</sub>	Cobalt ferrite
CTAB	Cetyl trimethylammonium bromide
DLS	Dynamic light scattering
DMF	Dimethyl formamide
DMSO	Dimethyl sulfoxide
DMEM	Dulbecco's Modified Eagle's medium (cell cultures)
DNA	Deoxyribonucleic acid
DOX	Doxorubicin
EDBE	(2,2-(ethylenedioxy)bisethylamine
EDC	1-Ethyl-3-(3-dimethylaminopropyl)carbodiimide
EDTA	Ethylenediaminetetraacetic acid
EGFR	Epidermal growth factor receptor
EPR	Enhanced permeation and retention effect
EtOH	Ethanol
Et <sub>2</sub> O	Diethyl ether
FACS	Fluorescence Activated Cell Sorting (in this)
FeCo	Iron cobalt alloy
FePt	Iron platinum alloy
FeO	Wustite
FDA	Food and drug Administration
FBS	Fetal bovine serum
Fe <sub>3</sub> O <sub>4</sub>	Magnetite
γ-Fe <sub>2</sub> O <sub>3</sub>	Maghemite
FITC	Fluorescein isothiocyanate
FT-IR	Fourier Transform Infra-Red spectra
g	Grams
Gd <sub>2</sub> O <sub>3</sub>	Gadolinium oxide
Gd-DOTA	Gd-tetraazacyclododecanetetraacetic acid
Gd-DTPA	Gd-diethylenetriamine pentaacetate
GdF <sub>3</sub>	Gadolinium fluoride
GdPO <sub>4</sub>	Gadolinium phosphate
<i>H</i>	Magnetic field
<i>H<sub>c</sub></i>	Coercive field
HCl	Hydrochloric acid
HER2	Human Epidermal growth factor receptor 2
HSA	Human serum albumin
IBD	Inflammatory bowel disease
IPTES	3-isocyanatopropyl triethoxy silane
ICAM1	Intercellular adhesion molecule 1
IONPS	Iron oxide nanoparticles
IACUC	Institutional Animal Care and Use Committee
K	Kelvin (unit for temperature)
K <sub>u</sub>	Anisotropy constant
MAdCAM1	Mucosal vascular addressin cell adhesion molecule 1
mAb	Monoclonal antibody
mg	Milligrams
μg	Micrograms

mM	Millimolar concentration
$\mu$ M	Micromolar concentration
MCF7	Michigan Cancer Foundation-7; HER2 positive breast cancer cell line
MEMRI	Manganese-enhanced MRI
MeOH	Methanol
MPIO	Paramagnetic iron oxide nanoparticles of micrometric size
MNPs	Magnetic nanoparticles
Mn-DPDP	Mangafodipirtrisodium
$\text{MnFe}_2\text{O}_4$	Manganese ferrite
MnO	Manganese oxide
MRI	Magnetic resonance imaging
MTT	3-(4,5-dimethylthiazol-2-yl)-2,5-diphenyltetrazolium bromide
MPH	Magnetic particle hyperthermia
$M_s$	Saturation magnetization
$M_R$	Remanent magnetization
$M_z$	Net Magnetization
NaOH	Sodium hydroxide
NSF	Nephrogenic systemic fibrosis
NHS	<i>N</i> -hydroxysuccinimide
NMR	Nuclear magnetic resonance
NaH	Sodium hydride
NPs	Nanoparticles
NTA	Nitrilotriacetic acid
NUS	National University of Singapore
PBS	Phosphate buffer solution
PEG	Poly ethylene glycol
PLGA	Poly(lactide-co-glycolide) acid
PMA	Poly(isobutylene- <i>alt</i> -maleic anhydride)
PVP	Polyvinyl pyrrolidone
RNA	Ribonucleic acid
RES	Reticulo endothelial system
$r_{SP}$	Superparamagnetic radius
RF	Radio frequency
RT	Room temperature
$\sigma$	Polidispersity
SAR	Specific absorption rate
SBB	Sodium borate buffer
scFV	Portion of the whole antibody
SBIC	Singapore Bioimaging Consortium
SEM	Scanning electron microscopy
SLP	Specific loss power
SPIO	Super paramagnetic iron oxide nanoparticles
SPDP	3-(2-pyridyldithio)propionate
TE	Echo time
TEM	Transmission electron microscopy
TEOS	Tetraethyl orthosilicate
THF	Tetrahydrofurane
TR	Repetition time
TZ	Trastuzumab moloclonal antibody
$T_1$	Longitudinal relaxation
$T_2$	Trasversal relaxation
USPIO	Ultra small superparamagnetic iron oxide nanoparticles
U87MG	Human primary glioblastoma cell line
VEGF	Vascular endothelial growth factor
Vs.	Versus

## **Acknowledgements**

I would like to thank all the people who made possible this work, for their support and encouragement during these years. First of all, my gratitude goes to my supervisor, Dr. Davide Prospero, for opening the doors of the NanoBioLab and giving me the opportunity of working with him and with all the wonderful persons who take part of his team; for being my mentor and for supporting me all the time.

Special thanks to Dr. Kai-Hsiang Chuang and Dr. Prashant Chandrasekharan, from SBIC, for giving me the tools to widen my skills in MRI during my stay in Singapore.

Thanks to the persons who collaborated and contributed with this work; all the team from Luigi Sacco Hospital and Nerviano Medical Sciences in Milan, and all the people from Prof. Ding's lab at the National University of Singapore.

Last, but not least, many thanks to my lovely family and friends for their support, for being there all the time and for making this adventure a more bearable experience.

## ABSTRACT

Inorganic nanoparticles have been extensively used in biomedical applications as a result of their electronic, optical, and magnetic properties that are derived from their nanometer size and composition. Their magnetic characteristics are crucial for the successful performance in applications such as magnetic resonance imaging (MRI), drug delivery, cellular signaling, and hyperthermia. MRI is one of the most powerful imaging techniques for living organisms as it provides images with excellent anatomical details based on soft-tissue contrast and functional information in a non-invasive and real-time monitoring manner. Among the different kinds of contrast agents currently available for clinical diagnosis, Gd-based contrast agents, specifically Gd (III) chelates, are used as positive magnetic resonance imaging (MRI) contrast agent. However, they generally induce the risk of nephrogenic systemic fibrosis (NSF) due to the dissociated  $Gd^{3+}$  ions from Gd (III) chelates. To avoid this problem, novel positive MRI contrast agents based on MnO have been developed, allowing low toxicity, high sensitivity, and active targeting when conjugated with biomolecules (antibodies).

During this work, the synthesis and characterization of MnO nanoparticles as positive contrast agents ( $T_1$ ) for MRI were carried out. Differences in size and morphology (round, star-like, cubic) were found by varying the reaction parameters such as solvent, temperature and reaction time. In order to determine their contrast enhancement,  $T_1$ -weighted images were acquired *in vitro* at different concentrations. Furthermore, to study their biocompatibility, up-take and proliferation assays were done in culture of endothelial cells SVEC4-1. To assess their biodistribution and wash out time, studies *in vivo* were carried out using a colitis induced murine model with 3% Dextran Sodium Sulfate (DSS) in drinking water. Data acquired showed a selective accumulation to inflammatory site in a short time suggesting a potential applicability for the diagnosis of the Inflammatory Bowel Disease (IBD).

Regarding the use of nanoparticles for hyperthermia, it's well known that the conversion of electromagnetic energy into heat by nanoparticles has the potential to be a powerful, non-invasive technique for biotechnology applications but poor conversion efficiencies have hindered practical applications so far. However, it has been demonstrated that it's possible to reach a significant increase in the efficiency of magnetic thermal induction by nanoparticles taking advantage of the exchange coupling between a magnetically hard core and magnetically soft shell to tune the magnetic properties of the nanoparticle and maximize the specific loss power.

For that reason, in an attempt to develop nanoparticles with high thermal energy transfer capability, during my internship at the Singapore Bioimaging Consortium (SBIC) and in collaboration with NUS, it was carried out a project to assess the thermal efficiency of Gd doped iron oxide nanoparticles. By using MRI,  $T_1$  maps were obtained using a turbo-spin echo inversion-recovery sequence with respiration gating. Biodistribution experiments were carried out and subsequently, ion concentration in organs of interest (liver, spleen, kidneys) and tumor were measured *ex vivo* by using ICP-MS technique. Finally, changes in temperature and Specific Absorption Rate (SAR) were determined in order to establish their thermal efficiency. Results obtained showed these novel nanoparticles can be used as a promising tool for diagnosis (MRI) and treatment (hyperthermia) of cancer tumors.

## List of publications

1. P. Verderio, S. Avvakumova, G. Alessio, M. Bellini, M. Colombo, E. Galbiati, S. Mazzucchelli, **J. Peñaranda Avila**, B. Santini, D. Prospero. *Delivering colloidal nanoparticles to mammalian cells: a nano-bio interface perspective*. Adv. Healthcare Mat. 2014, **3**(7): 957-976.
2. E. Cova, M. Colombo, S. Inghilleri, M. Morosini, S. Miserere, **J. Peñaranda-Avila**, B. Santini, D. Piloni, S. Magni, F. Gramatica, D. Prospero, F. Meloni. *Antibody-engineered nanoparticles selectively inhibit mesenchymal cells isolated from patients with chronic lung allograft rejection*. Nanomedicine 2015, **10**(1): 9-23.
3. S. Sommaruga, E. Galbiati, **J. Peñaranda-Avila**, C. Brambilla, P. Tortora, M. Colomobo, D. Prospero. *Immobilization of carboxypeptidase from *Sulfolobus solfataricus* on magnetic nanoparticles improves enzyme stability and functionality in organic media*. BMC Biotech. 2014, **14**(1): 82.



First section

## CONTENT

<b>Chapter I. Inorganic nanoparticles</b>	4
1.1. Introduction	4
1.2. Magnetic nanoparticles	5
1.2.1. M–H curves	6
1.3. Iron oxide nanoparticles	8
1.3.1. Synthesis of iron oxide nanoparticles	9
1.3.1.1. Coprecipitation	10
1.3.1.2. Aerosol-vapor technology	10
1.3.1.3. Solvothermal decomposition from organo-metallic precursors	11
1.3.2. Applications of Iron Oxide Nanoparticles in Biomedical Research	12
1.3.2.1. Drug delivery	12
1.3.2.2. Nanosensors	13
1.3.2.3. Magnetic Resonance Imaging (MRI): T <sub>2</sub> and T <sub>1</sub> contrast agent	13
1.3.2.4. Hyperthermia	14
1.4. Manganese oxide nanoparticles	15
1.4.1. Synthesis of manganese oxide nanoparticles	15
1.4.2. Applications of Manganese oxide Nanoparticles in Biomedical Research	16
<b>Chapter II. Magnetic resonance imaging</b>	24
2.1. Relaxation times T <sub>1</sub> and T <sub>2</sub>	26
2.1.1. T <sub>1</sub> -weighted images and Repetition Time (TR)	29
2.1.2. T <sub>2</sub> -weighted images and echo time (TE)	29
2.1.3. Magnetic Susceptibility	30
2.2. MRI contrast agents based on magnetic nanoparticles	31
2.2.1 Surface biocompatibility	32
2.3. T <sub>2</sub> contrast agents	36
2.3.1. Nanostructured T <sub>2</sub> contrast agents with improved magnetic properties	39
2.3.2. Multifunctional T <sub>2</sub> contrast agents	41
2.4. T <sub>1</sub> contrast agents	43
2.4.1 Gadolinium based contrast agents	45
2.4.2 New contrast agents based on Manganese	46
2.5. Application of MnO NPs for early diagnosis of Inflammatory Bowel Disease (IBD)	49

# Chapter I

---

## CHAPTER I

### INORGANIC NANOPARTICLES

#### 1.1. Introduction

The nanoscale, defined by the US National Nanotechnology Initiative, is a range from 1 to 1000 nm, including particles which are naturally occurring, such as particles in smoke, volcanic ash, sea spray, and from anthropogenic sources. In terms of biology, the nanoscale is the size range of important cellular components, such as double-stranded DNA (about 2.5 nm in diameter), proteins (hemoglobin is about 5 nm in diameter), cell walls, cell membranes, and compartments.<sup>[1]</sup> The SI prefix “nano” means a billionth ( $10^{-9}$ ) part of a meter, or about one hundred thousandth the thickness of a sheet of paper.

Metal nanoparticles have a long history in terms of preparation, characterization, and application. Understanding and exploring their properties and potential applications are major driving forces behind the synthesis of a large variety of functional nanomaterials. Many of these properties arise from their large surface-area-to-volume ratio and the spatial confinement of electrons, phonons, and electric fields in and around the particles. These may cause deviations from the usual bulk atomic arrangements, such as higher reactivity; different elastic, tensile, and magnetic properties; increased conductivity; or increased tendency to reflect and refract light.<sup>[2]</sup>

Nanoparticle research has been exploited to the use of inorganic nanoparticles in different technological fields; particularly, a significant factor is the development of a great number of applications in biomedical science, ranging from imaging to biochemical sensing, targeting and drug delivery.<sup>[3-9]</sup>

The main advantage of inorganic nanoparticles is attributed to their intrinsic physical properties including size dependent optical, magnetic, electronic, and catalytic properties as well as some biological activities (*e.g.* anti-bacteria or specific interactions).<sup>[10]</sup> In addition, the possibility of assembling inorganic nanoparticles, as physical supports, with biochemical building blocks lead to a broad selection of novel hybrid systems with interesting properties, thus allowing to reveal more elaborate structures, which are expected to expand further the range of biomedical applications of inorganic nanomaterials.<sup>[11]</sup> The main challenge of these chemical approaches is the controlled synthesis of nanostructures such that they are uniform in size, shape, chemical composition, they are produced in high yields, and they are stable in biological environments.

Moreover, many functional groups providing a wide range of potential interactions between organic moieties and biomolecules with nanoparticle surface can be easily used to compose a bio-nano structure with a specific biological function.<sup>[2]</sup> Thus, the modification of peptides, proteins and other complex molecules with specific anchoring groups facilitates the binding to nanoparticles *via* a site-specific linkage, introducing chemical functionalities that can provide recognition of antibodies or cell receptors.<sup>[12]</sup> Understanding the profile of the biomolecule-nanoparticle interactions at their interface and with biological systems such as cells and tissues is crucial as it may affect the structures at the molecular level thus affecting their biological function or application. For that reason, design and optimization of effective functionalization strategies are critical to ensure the success of these nano-bio systems.<sup>[2]</sup>

The present chapter focuses on describing some inorganic magnetic nanoparticles, specifically those based on iron (Fe) and manganese (Mn), which are promising for biomedical applications due to their fascinating properties. Different synthetic approaches of these nanoparticles will also be mentioned as well as their surface modifications with organic and active biomolecules.

## 1.2. Magnetic nanoparticles

Magnetic nanoparticles offer some attractive possibilities in biomedicine as they have controllable sizes ranging from a few nanometres up to tens of nanometres, which places them at dimensions that are smaller than or comparable to those of a cell (10–100 $\mu$ m), a virus (20–450 nm), a protein (5–50 nm) or a gene (2 nm wide and 10–100 nm long).<sup>[13]</sup> Moreover, their capability of being manipulated under an external magnetic field provide controllable means of magnetically tagging biomolecules, leading to potentially highly efficient bioseparation, highly sensitive biosensing and magnetic resonance imaging (MRI) contrast enhancement, as well as site-specific drug delivery.<sup>[14]</sup> At the same time, due to their resonantly response to an alternating magnetic field, allow the transfer of magnetic energy to the particles as a form of heat, opening up the possibility of being used as a key approach to successful cancer therapy in the future.

For biomedical applications, it is required that magnetic nanoparticles to be monodisperse so that each individual nanoparticle has nearly identical physical and chemical properties for controlled biodistribution, bioelimination and contrast effects. They should also have high magnetic moment, and can be modified via surface chemistry reactions so that they are capable of binding specifically to the biomolecules of interest and able to resist different physiological conditions.<sup>[14]</sup>

### 1.2.1. M–H curves

Under the presence of a magnetic field of strength  $\mathbf{H}$ , the individual atomic moments of a magnetic material contribute to its overall response so that the magnetic induction is defined by:

$$\mathbf{B} = \mu_0(\mathbf{H} + \mathbf{M}), \text{ eq. (1)}$$

where  $\mu_0$  is the permeability of free space, and the magnetization  $\mathbf{M} = \mathbf{m}/V$  is the magnetic moment per unit volume, where  $\mathbf{m}$  is the magnetic moment on a volume  $V$  of the material.<sup>[13]</sup>

Since all materials are magnetic to some extent, with their response depending on their atomic structure and temperature, they may be conveniently classified in terms of their volumetric magnetic susceptibility,  $\chi$ , where

$$\mathbf{M} = \chi\mathbf{H}, \text{ eq. (2)}$$

describes the magnetization induced in a material by  $\mathbf{H}$ . In SI units  $\chi$  is dimensionless and both  $\mathbf{M}$  and  $\mathbf{H}$  are expressed in  $\text{Am}^{-1}$ . The susceptibility in ordered materials depends not just on temperature, but also on  $\mathbf{H}$ , which gives rise to the characteristic sigmoidal shape of the M–H curve, with  $\mathbf{M}$  approaching a saturation value at large values of  $\mathbf{H}$  (Fig 1.1. a).

Magnetic materials are characterized by the presence of magnetic dipoles generated by the spinning of some of their electrons. Each of these polarized electrons can be aligned in a parallel or anti-parallel fashion with respect to the neighboring ones in the crystal lattice and this type of interaction is what gives rise to the macroscopic magnetic effect that we can measure. Depending on the magnetic response observed, it is possible to classify magnetic materials as *paramagnets*, *ferromagnets*, *ferrimagnets* or *anti-ferromagnet*.<sup>[15]</sup>

*Paramagnetic* materials are characterized by uncouple (randomly oriented) magnetic dipoles, which can be aligned only in the presence of an external magnetic field and along its direction. This type of material has no coercivity nor remanence, which means that when the external magnetic field is switched off, the internal magnetic dipoles randomize again, no extra energy is required to demagnetize the material and hence the initial zero net magnetic moment is spontaneously recovered.<sup>[2]</sup>

In the other hand, materials exhibiting an enhanced collective response even in the absence of an external magnetic field are known as *ferromagnetic*. This phenomenon is due to the parallel alignment of single magnetic dipoles in a crystal. When it occurs, the strength and magnetization of the materials can be described by three main parameters (Fig. 1.1.a):<sup>[15]</sup>

(a) *Coercive Field ( $H_C$ )*: is the external field of opposite sign required to reduce the magnetization back to zero. It represents also the minimum energy required for the reversal of the magnetization of the material.  $H_C$  is strictly related to the magnetic anisotropy constant ( $K_u$ ) that determines the energy to be overcome in order to invert the direction of the magnetic dipoles of the material and can have different contributions such as the symmetry of the crystal lattice, the surface contribution with respect to the core of the nanoparticle, and finally the shape of the nanoparticle.<sup>[15]</sup>

(b) *Saturation Magnetization ( $M_S$ )*: is the maximum value of magnetization that the material can reach under the effect of sufficiently high magnetic fields.

(c) *Remanent Magnetization ( $M_R$ )*: indicates the residual magnetization at zero applied field.

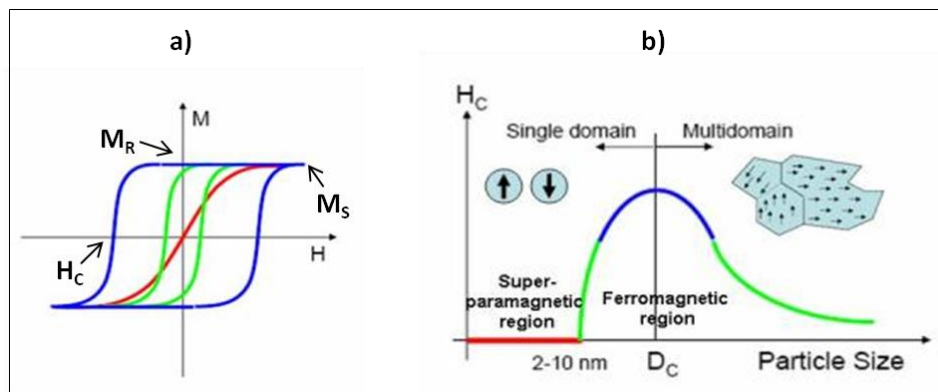


**Figure 1.1:** a) Theoretical magnetization ( $M$ ) versus magnetic field ( $H$ ) for different materials: Depending on the particle size, materials exhibit either a multi-domain (green), single-domain (blue) or superparamagnetic (red) behavior. b) Variation of the coercivity ( $H_C$ ) of magnetic nanoparticles with size.

In materials where neighboring magnetic dipoles align anti-parallel in the lattice, thus repulsing each other, the magnetic exchange can lead to two different phenomena called *anti-ferromagnetism* and *ferrimagnetism*. The former case occurs when the magnetic dipoles or interacting spins have the same value and hence the material shows a net zero magnetization. In the latter, the two coupled spins show different values so that the net magnetic dipole different than zero will still magnetize the material even in the absence of an external magnetic field.

Ferromagnetic and ferrimagnetic materials show irreversibility in the magnetization process related to the pinning of magnetic domain walls at impurities or grain boundaries within the material, as well as to intrinsic effects such as the magnetic anisotropy of the crystalline lattice. This gives rise to open M–H curves, called hysteresis loops.

To overcome the barrier to domain wall motion in these materials, energy is needed. This energy is delivered by the applied field, and can be characterized by the area enclosed by the hysteresis loop. This leads to the concept that applying a time-varying magnetic field to a ferromagnetic or ferrimagnetic material, it is possible to establish a constant flow of energy into that material, which will be transferred into thermal energy.<sup>[13]</sup> The shape of these loops are determined in part by particle size: in large particles (of the order micron size or more) there is a multi-domain ground state which leads to a narrow hysteresis loop since it takes relatively little field energy to make the domain walls move; while in smaller particles there is a single domain ground state which leads to a broad hysteresis loop.<sup>[13]</sup> A further reduction of the size below a certain value of the radius (called superparamagnetic radius,  $r_{SP}$ ), induces a magnetic transition in particles where both ferro and ferrimagnetic nanoparticles become *superparamagnetic*. This behavior is strictly associated to nanoformed magnetic materials and arises when the thermal energy is sufficiently high to overcome the magnetic stabilization energy of the particle (Fig 1.1.b).<sup>[15]</sup>

The size reduction of magnetic materials shows enhancing advantages that make them more suitable for therapeutic and diagnostic techniques compared to their bulk counterparts; for example magnetic parameters such as the  $H_C$  of particles can be tuned by decreasing their size and, consequently, the biomedical performance of the sample can be optimized to the practical requirements. This last property translates into a considerable advantage, especially for *in vivo* experiments: the absence of  $H_C$  (the zero net magnetic moment) of the nanoparticles after concluding the diagnostic measurement will prevent the potential aggregation of MNPs that could easily cause the formation of embolisms in the blood vessels.<sup>[2]</sup>

### 1.3. Iron oxide nanoparticles

Iron is one of the most abundant metallic elements in living organisms, and is essential for various biological processes, such as oxygen transport by hemoglobin and cellular respiration by redox enzymes.

Iron oxide nanoparticles (IONPs), which are usually magnetic susceptible, are one of the few nanomaterials that can be injected into the body and incorporated into natural metabolic pathways of human body; for these reasons, compared with many other nanoparticles, iron oxide nanoparticles are less toxic and more biologically tolerated in a broad range of concentrations.<sup>[2]</sup>



The application of small iron oxide particles in *in vitro* diagnostics has been practised for nearly 40 years. In the last decade, increased investigations with several types of iron oxides have been carried out in the field of nanosized magnetic particles (mostly maghemite,  $\gamma$ -Fe<sub>2</sub>O<sub>3</sub>, or magnetite, Fe<sub>3</sub>O<sub>4</sub>, single domains of about 5–20 nm in diameter), among which magnetite is a very promising candidate since its biocompatibility has been already proven [16]. IONPs doped with magnetically susceptible elements (*e.g.* MnFe<sub>2</sub>O<sub>4</sub> and CoFe<sub>2</sub>O<sub>4</sub>) and metal alloys nanoparticles (*e.g.* FeCo and FePt) are also available, but they are much less employed in biomedical applications because of their potential toxicity and rapid oxidation, even though the magnetism of these ferrites and metal alloys is stronger than that of the corresponding pure iron oxide.<sup>[2]</sup>

The metabolism and pharmacokinetics of intravenously injected IONPs have been well studied and, in addition to their superior biocompatibility, they offer many important advantages for biomedical applications, such as MRI contrast enhancement, tissue repair, immunoassays, detoxification of biological fluids, hyperthermia, drug delivery and cell separation.<sup>[17]</sup> All of these applications require that the nanoparticles have high magnetization values, a size smaller than 100 nm, and a narrow particle size distribution. Moreover, the surface coating of these nanoparticles has to be nontoxic and biocompatible and must also allow for a targetable delivery with particle localization in a specific area. Such magnetic nanoparticles can bind to drugs, proteins, enzymes, antibodies, or nucleotides and can be directed to an organ, tissue, or tumor using an external magnetic field.<sup>[18]</sup> Currently, there are some iron oxide nanoparticle-based MR contrast agents that have already been used in clinical trials, or are undergoing clinical trials<sup>[19]</sup>. Most of them are covered by a specific organic and/or inorganic layer. Their appropriate coating depends on the type of nanoparticle core and the proposed applications since differently coated iron oxide nanoparticles will have different effects on cells and different fates in the body. Hence, the suitable chemical design of both the core and shell of the nanoparticle is extremely important for future projected clinical practice.<sup>[20]</sup>

### 1.3.1. Synthesis of iron oxide nanoparticles

A great number of physical and chemical methods have been applied to synthesize MNPs.<sup>[21]</sup> Physical methods are advantageous due to they allow mass production and high-purity nanomaterials can be obtained, but it is difficult to control the size and shape of the nanoparticles.<sup>[22]</sup>

To overcome these drawbacks, various chemical methods based on solution-phase colloidal chemistry have been investigated for the synthesis of high quality nanoparticles. These chemical methods include metal salt reduction, sol-gel process, reverse micelle technique, and thermal decomposition of iron organic precursors.<sup>[23]</sup> Nevertheless, to prepare iron oxide nanoparticles suitable for the intended medical applications, the use of “green chemistry” is highly recommended, which avoids the use of toxic chemicals. It is also desirable to have a synthetic process that is scalable to industrial applications, and should be reproducible from batch to batch. A briefly description of the most representative methods for the scalable synthesis of iron oxide nanoparticles for medical use is described below.

#### *1.3.1.1 - Coprecipitation*

Magnetite is prepared by reacting Fe(II) and Fe(III) salts in alkaline aqueous media in a molar ratio of 1:2. Nanoparticles made by this method could be used for biomedical applications because of their easy and large-scale production; and their direct dispersion in water without further treatment.<sup>[24]</sup> However, the synthesized magnetite particles from this process are highly polydisperse and unstable. To further improve their stability, iron oxide nanoparticles were coated in situ using various capping ligands such as hydroxamate, dimercaptosuccinic acid, phosphorylcholine, and citric acid.<sup>[25, 26]</sup> However, the crystallinity of the synthesized iron oxide nanoparticles is very poor, which reduces their magnetic susceptibility.

#### *1.3.1.2- Aerosol-vapor technology*

The aerosol/vapor technology (*e.g.* flame-spray, laser pyrolysis) is used to produce a wide range of iron oxide nanoparticles such as magnetite, maghemite, and wustite (FeO), which can be controlled by varying the fuel-to-air ratio during combustion, as well as by controlling the valence state of the iron precursors, with size ranging from 2 to 7 nm depending on the pyrolysis conditions.<sup>[2]</sup> In flame-spray pyrolysis, ferric salt and reducing agent, mixed together in an organic solvent, are sprayed into a series of reactors to condense the aerosol solute, followed by evaporating the solvent.<sup>[27]</sup> In laser pyrolysis, a laser is used to heat a gaseous mixture of an iron precursor and a flowing mixture of gases in order to produce well-dispersed fine nanoparticles.<sup>[28]</sup> Unfortunately, because of the difficulty of obtaining a uniform size for the initial droplets or gaseous mixture, the final nanoparticles made by this process have a very broad size distribution.

### 1.3.1.3- Solvothermal decomposition from organo-metallic precursors

Highly uniform-disperse IONPs can be synthesized on a large scale by solvothermal decomposition of organometallic iron precursor such as iron pentacarbonyl, iron cupferron, iron oleate, or iron acetylacetonate in a hot surfactant solution.<sup>[29-33]</sup> Nanoparticles synthesized by solvothermal decomposition have high crystallinity and uniform size distribution with polydispersity ( $\sigma$ )  $\approx$  10%. Hyeon et al. reported the fabrication of highly uniform iron oxide nanoparticles by the thermal decomposition of iron oleate complex, which was prepared by the reaction of iron pentacarbonyl with oleic acid.<sup>[29]</sup> Monodisperse iron oxide nanoparticles were obtained by mixing iron pentacarbonyl precursor with oleic acid solution at low temperature and heating up the reaction mixture to high temperature. The size of the nanoparticles was controlled by adjusting the molar ratio of iron pentacarbonyl to oleic acid. Few years later it was reported a synthetic method of obtaining mono-disperse IONPs using an inexpensive and nontoxic iron chloride ( $\text{FeCl}_3$ ) rather than toxic and expensive iron pentacarbonyl,<sup>[34]</sup> (Figure. 1.2).

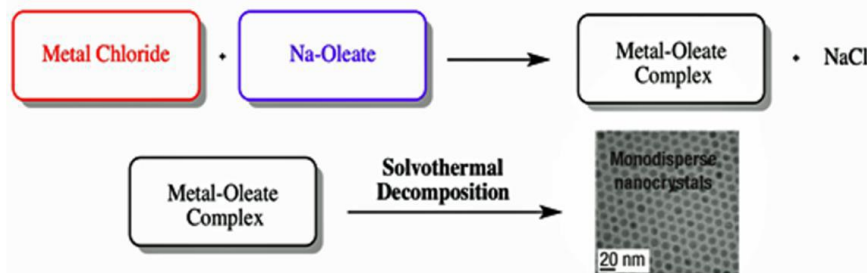


**Figure 1.2:** Scheme for the ultra-large-scale synthesis of monodisperse nanocrystals.

A dispersion containing the iron-oleate complex, generated from the reaction between  $\text{FeCl}_3$  and sodium-oleate, is soaked in a high boiling solvent (1- octadecene); the mixture is slowly heated to the boiling point of the solvent to produce the mono-disperse nanoparticles. The size of the iron oxide nanoparticles may be modulated by changing the aging temperature. When 1-hexadecene [boiling point (bp): 274 °C], octyl ether (bp: 287 °C), 1- octadecene (bp: 317 °C), 1- eicosene (bp: 330 °C), and trioctylamine (bp: 365 °C) were used as the solvent, 5-nm, 9-nm, 12-nm, 16-nm, and 22-nm iron oxide nanoparticles have been produced, respectively.<sup>[2, 35-37]</sup> Very recently, uniform and extremely small iron oxide nanoparticles of less than 4 nm have been synthesized via the thermal decomposition of an iron–oleate complex in the presence of oleyl alcohol. The use of oleyl alcohol reduced the reaction temperature by reducing the iron– oleate complex, resulting in the production of extremely small IONPs.

This size could be finely controlled from 1.5 nm to 3.7 nm by changing the ratio of oleyl alcohol to oleic acid or by changing the aging temperature.<sup>[2, 38]</sup>

### **1.3.2. Applications of Iron Oxide Nanoparticles in Biomedical Research**

Magnetic nanoparticles offer some attractive possibilities in biomedicine. Their controllable sizes ranging from a few nanometers up to tens of nanometers, places them at dimensions where they can ‘get close’ to a biological entity of interest. Indeed, they can be coated with biological molecules to make them interact with or bind to a biological entity, thereby providing a controllable means of ‘tagging’ or addressing it.<sup>[13]</sup> In this section four particular applications of IONP will be considered: drug delivery, nanosensors, magnetic resonance imaging (MRI) contrast enhancement and hyperthermia treatments.

#### *1.3.2.1- Drug delivery*

Magnetic iron oxide nanoparticle-based nanovectors have been intensively studied also as drug delivery vehicles; this immediately upgrades the MRI imaging probes to theranostic agents that combine both diagnostic and therapeutic elements.<sup>[10, 39, 40]</sup> One trick is to load IONPs, along with therapeutic agent, into polymer-based matrices.<sup>[41]</sup> Recently, Nasongkla et al. developed iron oxide nanoparticle-based theranostics, named SPIO-doxorubicin (Dox)-cRGD micelles for synchronous cancer imaging and traceable drug delivery.<sup>[42]</sup> This approach showed the therapeutic modality of Doxorubicin and the diagnostic features of the cluster of IONPs which has been co loaded into the cores of PEG-PLA micelles, while the targeting ligand, a cRGD peptide, has been attached onto the micelle surface for targeting the integrin  $\alpha v \beta 3$  overexpressed on tumor endothelial cells.

Aside from co-capsulation and/or chemical covalent coupling of drugs, therapeutics can also be loaded into hollow iron oxide nanoparticles via physical absorption.<sup>[43]</sup> For instance, the Sun group developed porous iron oxide nanoparticles with a sizable cavity by controlled oxidation and acid etching of Fe particles.<sup>[44]</sup> In this work the authors loaded cisplatin, a powerful therapeutic agent against numerous solid tumors, into the cavities of the nanoparticles, and coupled Trastuzumab, a monoclonal antibody that interferes with the HER2/neu receptor, onto the nanoparticle surfaces to confer targeting specificity; in this way the functionalized iron oxide nanoparticles showed a selective affinity to HER2 receptors, overexpressed on breast cancer cells, and a sustained toxicity attributable to the release of cisplatin from the nanoparticles.

### 1.3.2.2- Nanosensors

The magnetic properties and significant surface area to volume ratio of iron oxide nanoparticles offer desirable characteristics for biomarker detection. Generally, the controlled clustering or aggregation of a few superparamagnetic iron oxide nanoparticles can greatly shorten  $T_2$  relaxation time compared to single nanoparticles at the same iron concentration; thus, when magnetic nanosensors aggregate through affinity ligands to the biomarkers, a decrease in the  $T_2$  relaxation time is observed, allowing the sensitive and accurate detection of biomarkers with excellent temporal and spatial resolution.<sup>[45, 46]</sup>

El-Boubbou et al. developed a magnetic nanosensor bearing carbohydrates to screen the carbohydrate-binding characteristics of cancer cells by MRI.<sup>[47]</sup> The system consists of micro coils for radio-frequency excitation and signal detection, an on-board NMR spectrometer, a portable magnet, and micro-fluidic networks. Magnetic iron oxide nanoparticles were conjugated with antibodies to each biomarker, followed by incubation with samples of cancer cells. Significant differences in  $T_2$  relaxation time were observed for a variety of cancer cells using this system; in this way, this strategy with high sensitivity, specificity and high-throughput shows great potential for early cancer diagnosis in the clinic.<sup>[2]</sup>

At the same time, Colombo et al. reported the accurate and reliable detection of anti-HSA (human serum albumin) antibodies by protein-functionalized magnetic nano-spherical probes due to the reversible alteration of their micro aggregation state induced by protein antibody specific interaction, sensed as changes in the  $T_2$  relaxation time of surrounding water molecules.<sup>[48]</sup>

### 1.3.2.3- Magnetic Resonance Imaging (MRI): $T_2$ and $T_1$ contrast agent

The contrast enhancement in MRI occurs as a result of the interaction between the contrast agents and neighboring water protons, which can be affected by many intrinsic and extrinsic factors such as proton density and MRI pulse sequences. The basic principle of MRI is based on nuclear magnetic resonance (NMR) together with the relaxation of proton spins in a magnetic field.<sup>[49]</sup> When the nuclei of protons are exposed to a strong magnetic field, their spins align either parallel or anti-parallel to the magnetic field applied. After the disappearance of the RF pulse, the excited nuclei relax to their initial, lower-energy state.

There are two different relaxation pathways: the first, called longitudinal or  $T_1$  relaxation, and the second, called transverse or  $T_2$  relaxation. Based on their relaxation processes, the contrast agents are classified as  $T_1$  and  $T_2$  contrast agents. Commercially available  $T_1$  contrast agents are usually paramagnetic complexes, while  $T_2$  contrast agents are based on IONPs, which are the most representative nanoparticulate.<sup>[49]</sup> It is reported in Table.1.1 some examples of  $T_2$  contrast agents based on IONPs, commonly exploited in biomedical MRI. More detailed information regarding the use of nanoparticles as contrast agents for MRI can be found in chapter II.

Name	Core NPs	Surface	Diam (nm)	Magnetization [emu g <sup>-1</sup> ]	$r_2$ [mM <sup>-1</sup> s <sup>-1</sup> ]	$B_0$ applied [T]
Feridex	Fe <sub>3</sub> O <sub>4</sub>	Dextran	4.96	45	120	1.5
Resovist	Fe <sub>3</sub> O <sub>4</sub>	Carboxydextran	4	60	186	1.5
Combix	Fe <sub>3</sub> O <sub>4</sub>	Dextran	5.85	61	65	1.5
CLIO-Tat	Fe <sub>3</sub> O <sub>4</sub>	Dextran	5	60	62	1.5
MEIO	Fe <sub>3</sub> O <sub>4</sub>	DMSA	4	25	78	1.5

**Table. 1.1:** Commercially available  $T_2$  contrast agent based on iron oxide nanoparticles.

#### 1.3.2.4- Hyperthermia

Using magnetic nanoparticles, particularly those capable of being delivered selectively to a tumor, offer the potential to deliver site-selective, and even cell-specific, heat to the local or microscopic environment of a tumor. The underlying mechanism is that magnetic nanoparticles can act as antennae in an external alternating magnetic field to convert electromagnetic energy into heat. This feature holds promise in cancer therapy for cancer cells that are more susceptible to elevated temperature than normal cells. In the thermo-therapy, magnetic fluids containing IONPs are delivered to the tumor and then heated by external alternating magnetic field, resulting in an increase of the local temperature of cancer tissue.<sup>[50]</sup> In this sense, Zhao and co-workers have found that head and neck tumor cells in mice can be killed in half an hour without harming normal cells by injecting a IONPs solution directly into the tumor site under the presence of an alternating magnetic field.<sup>[51]</sup> In an analogue study aminosilane coated IONPs have been injected into a subcutaneous tumor model in rats, allowing raising the temperature of tumor above 43 °C and causing tumor regression when exposed to an alternating magnetic field.<sup>[52]</sup>

## 1.4. Manganese oxide nanoparticles

Manganese (Mn) is one of the most abundant elements in the biosphere. Manganese oxide nanoparticle systems are of interest for a variety of applications including catalysts and electronics. Their magnetic characteristics, like the observation of ferromagnetism in nanoparticulate MnO (which is otherwise a bulk antiferromagnet), have attracted substantial interest in the recent years.<sup>[53]</sup> The unique electronic configuration of the  $3d^5$  shell of  $Mn^{2+}$  makes it an excellent magnetic probe for applications in the biomedical field such as drug delivery and biomedical imaging as an MRI contrast agent.<sup>[54]</sup> Indeed, some colloidal nanoparticles containing manganese (II) have recently been reported as contrast agents for MRI.

Manganese possesses five unpaired electrons, and the spin of them in manganese perturbs the relaxation of proton in water molecules, which results in an efficient shortening of longitudinal relaxation time, and hence increases the intensity of magnetic resonance signal.

The recent development of molecular and cellular imaging to help visualize disease-specific biomarkers at the molecular and cellular levels has led to an increased interest in magnetic nanoparticles as MRI contrast agents. In particular, superparamagnetic iron oxide (SPIO) has emerged as the prevailing agent so far. However, their negative contrast effect and magnetic susceptibility artifacts are significant drawbacks of using SPIO in MRI. The resulting dark signal can mislead the clinical diagnosis in  $T_2$ -weighted MRI because the signal is often confused with the signals from bleeding, calcification, or metal deposits and the susceptibility artifacts distort the background image.<sup>[55]</sup> In comparison with SPIO, the MnO nanoparticles contribute bright field of  $T_1$ -weighted MRI, which can be more easily distinguished as they enhance signal instead of reducing it. As a result, the application of the MnO nanoparticles as contrast agent of MRI has gained considerable attention.<sup>[56]</sup>

### 1.4.1. Synthesis of manganese oxide nanoparticles

Thermal decomposition has been one of the most widely used and reliable routes to produce relatively large batches of small and narrow particle size distributions. More recently, one-pot synthesis techniques have also been developed in high boiling point solvents, enabling the production of 1–3 nm diameter particles.<sup>[57]</sup> After synthesis, the particles are covered with ligands or polymers, and suspended in water to measure their hydrodynamic sizes and properties as MRI contrast agents.

For this, both the transverse and longitudinal relaxation rates ( $1/T_2$  and  $1/T_1$ ) are measured, and plotted as a function of the Mn concentration values to calculate their relaxivities ( $r_2$  and  $r_1$ ). The potential of a positive ( $T_1$ ) contrast agent for MRI can be established by high  $r_1$  values and  $r_2/r_1$  values as close as possible to 1.

One of the first studies regarding MnO nanoparticles, performed by Na et al, revealed the strong dependence of the nanoparticle core surface on the longitudinal relaxivity.<sup>[55]</sup> They developed PEG–lipid-coated MnO nanoparticles with core diameters ranging from 7–25 nm. Unfortunately, very low longitudinal relaxivities were found ( $r_1 = 0.37 \text{ mM}^{-1} \text{ s}^{-1}$  and  $r_2/r_1 = 4.7$  for 7 nm diameter MnO nanocrystals at 3 T). The rather low relaxivities nonetheless were used to label and to track rat glioma cells in vivo, using  $T_1$ -weighted imaging sequences. Then, hollow MnO particles with a  $\sim 25$  nm thick porous silica shell were designed as high stability cell tracking imaging probes.<sup>[58]</sup> Compared with the latter, the longitudinal relaxivity of these particles appeared slightly increased ( $r_1 = 0.99 \text{ mM}^{-1} \text{ s}^{-1}$  at 11.7 T), allowing the tracking of mesenchymal stem cells over a period of at least 14 days. However, the longitudinal relaxivity of these suspensions was still four (4) to ten (10) times lower than that observed for common clinical contrast agents such as Gd-DTPA and Gd-DOTA. In fact, coating MnO particles with a layer of silica considerably affects optimal water exchange between the matrix and the surface paramagnetic ions, which is a key mechanism guaranteeing the performance of this kind of MRI contrast agents.<sup>[57]</sup> Although  $\text{Mn}^{2+}$  ions are paramagnetic, MnO nanoparticles in the range 5–10 nm express an antiferromagnetic behaviour. The most significant increase in relaxivity was reported for MnO particles synthesized using polyol techniques ( $r_1 = 7.75$  at 1.5 T, for PEG-coated MnO particles). However, the relaxometric ratio of these particles was close to that of Mn ions ( $r_2/r_1 = 10$ ), revealing the possible degradation of MnO cores upon complexation with carboxylic ligands. Indeed, aqueous  $\text{Mn}^{2+}$  solutions show relaxivities in the order of  $r_1 = 5.2 \text{ mM}^{-1} \text{ s}^{-1}$  and  $r_2 = 61 \text{ mM}^{-1} \text{ s}^{-1}$  at 1.41 Tesla and 25 °C. Hence, the coating strategies are important to provide enhanced colloidal stability, with possible improvement on the chemical stability of MnO nanoparticles.<sup>[57]</sup>

#### **1.4.2. Applications of Manganese oxide Nanoparticles in Biomedical Research**

The use of Manganese based nanoparticles in the biomedical field has been focused in their application as positive contrast agents for MRI.



Current MRI contrast agents are in the form of either paramagnetic complexes or magnetic nanoparticles. Paramagnetic complexes, which are usually gadolinium ( $\text{Gd}^{3+}$ ) or manganese ( $\text{Mn}^{2+}$ ) chelates, accelerate longitudinal ( $T_1$ ) relaxation of water protons and exert bright contrast in regions where the complexes localize. For instance, gadolinium diethylenetriamine pentaacetate (Gd-DTPA) has been the most widely used of such complexes and its main clinical applications are focused on detecting the breakage of the blood-brain barrier (BBB) and changes in vascularity, flow dynamics, and perfusion. Manganese-enhanced MRI (MEMRI), which uses manganese ion ( $\text{Mn}^{2+}$ ) as a  $T_1$  contrast agent, is applicable to animals only owing to the toxicity of  $\text{Mn}^{2+}$  when it accumulates excessively in tissues and despite the increasing appreciation of this technique in neuroscience research.<sup>[55]</sup>

The most commonly used positive ( $T_1$ -weighted) contrast agent in clinic is gadolinium chelates, such as the popular Gd-diethylenetriamine pentaacetate (Gd-DTPA) and Gd-tetraazacyclododecanetetraacetic acid (Gd-DOTA). However, the dissociated gadolinium ions from gadolinium chelates could induce the risk of nephrogenic systemic fibrosis (NSF).<sup>[59]</sup> Thus, many strategies, such as the loading of macromolecules and micelles, the fabrication of nanoscale objects, and so on, have been attempted to inhibit the toxicity and side-effect of released gadolinium ions together with retaining good contrast effect. Especially, the application of inorganic nanoparticles as contrast agent of MRI has gained considerable attention due to relatively high stability and good MRI function. For example, gadolinium compound-based crystalline nanoparticles, such as the Gd-containing nanoparticles of  $\text{Gd}_2\text{O}_3$ ,  $\text{GdF}_3$  and  $\text{NaGdF}_4$ , provide a rigid crystal environment that is effectively prevent nanoparticles from releasing free gadolinium ions, and so that they have been mostly investigated as a new generation of positive contrast agents.<sup>[59]</sup> As mentioned before, the electronic configuration of manganese ions, which has five unpaired electron, results in an efficient shortening of longitudinal relaxation time of proton in water together with the enhancement of magnetic resonance signal intensity. Furthermore, the toxicity of manganese ions is much lower than that of gadolinium ions. As a result, the manganese compound-based crystalline nanoparticles, such as  $\text{MnO}$  nanoparticles, are expected to become potential positive contrast agents for  $T_1$ -weighted MRI. It is generally recognized that the predominant contrast effect is only contributed by the manganese near to the surface, which could be close contact with the proton of water molecules.

Therefore, it is essential to synthesize monodisperse ultrasmall MnO nanoparticles to provide large specific surface area for touching water molecules intimately. Since the as-synthesized MnO nanoparticles are generally hydrophobic, surface modification is attempted to render these MnO nanoparticles hydrophilic and more biocompatible.<sup>[59]</sup>

At present, there is one commercial Mn-based MRI contrast agent, mangafodipirtrisodium (Mn-DPDP), in clinical use. However, Mn-based complexes are easy to dissociate after administration to yield free Mn<sup>2+</sup> because of the conversion between the six- and seven-coordinated states, which accounts for the in vivo instability of the Mn-DPDP chelate compared with gadolinium-based contrast agents. Due to its physiological role, exposure to excess Mn can induce deleterious effects on the central nervous system and cause parkinsonism-like syndrome, especially in patients with liver failure. The in vivo instability of Mn-DPDP has raised especial concerns about its potential toxicity from the Mn<sup>2+</sup> ions, which led to its gradual withdrawing from the market. It also suggests that it is necessary to find biocompatible and thermodynamic stable Mn compounds.<sup>[54]</sup> With the tremendous advances in nanotechnology, some types of Mn-NPs-based MRI contrast agent with well defined morphology and high solubility have been developed. They exhibit favorable behaviors in detection, localization, characterization and evaluation of hepatic lesions and provide clinical advantages over the existing Mn-based MRI contrast agent, Mn-DPDP. Some of them have offered an improved biocompatible profile; however, the overall and systematic research on Mn-based nano-contrast agents is still at a relatively early stage.<sup>[54]</sup>

## REFERENCES

1. Sperling, R.A., et al., *Biological applications of gold nanoparticles*. Chemical Society Reviews, 2008. **37**(9): p. 1896-1908.
2. Verderio, P., *Synthesis and Biofunctionalization of Novel Composite Nanocarriers for Targeted Detection and Treatment of Malignant Cells*, in *Chemical Sciences* 2014, University of Milan Bicocca: Milan.
3. Ladj, R., et al., *Individual inorganic nanoparticles: preparation, functionalization and in vitro biomedical diagnostic applications*. Journal of Materials Chemistry B, 2013. **1**(10): p. 1381-1396.
4. Swierczewska, M., S. Lee, and X. Chen, *Inorganic nanoparticles for multimodal molecular imaging*. Molecular imaging, 2011. **10**(1): p. 3.
5. Peng, G., et al., *Diagnosing lung cancer in exhaled breath using gold nanoparticles*. Nature nanotechnology, 2009. **4**(10): p. 669-673.
6. Yeom, S.-H., et al., *Nanostructures in biosensor--a review*. Frontiers in bioscience (Landmark edition), 2010. **16**: p. 997-1023.
7. Na, H.B., I.C. Song, and T. Hyeon, *Inorganic nanoparticles for MRI contrast agents*. Advanced Materials, 2009. **21**(21): p. 2133-2148.
8. Tan, S., et al., *Lipid-enveloped hybrid nanoparticles for drug delivery*. Nanoscale, 2013. **5**(3): p. 860-872.
9. Kim, C.S., et al., *Inorganic nanosystems for therapeutic delivery: status and prospects*. Advanced drug delivery reviews, 2013. **65**(1): p. 93-99.
10. Huang, H.-C., et al., *Inorganic nanoparticles for cancer imaging and therapy*. Journal of controlled Release, 2011. **155**(3): p. 344-357.
11. Sapsford, K.E., et al., *Functionalizing nanoparticles with biological molecules: developing chemistries that facilitate nanotechnology*. Chemical reviews, 2013. **113**(3): p. 1904-2074.
12. Wilson, D.S., et al., *Orally delivered thioketal nanoparticles loaded with TNF- $\alpha$ -siRNA target inflammation and inhibit gene expression in the intestines*. Nature materials, 2010. **9**(11): p. 923-928.
13. Pankhurst, Q.A., et al., *Applications of magnetic nanoparticles in biomedicine*. Journal of Physics D: Applied Physics, 2003. **36**(13): p. R167.
14. Xu, C. and S. Sun, *Monodisperse magnetic nanoparticles for biomedical applications*. Polymer International, 2007. **56**(7): p. 821-826.
15. O'Handley, R.C., *Modern Magnetic Materials: Principles and Applications*. 2000: Wiley & Co. ©, New York (USA).
16. Gupta, A.K. and M. Gupta, *Synthesis and surface engineering of iron oxide nanoparticles for biomedical applications*. Biomaterials, 2005. **26**(18): p. 3995-4021.
17. Cho, H., et al., *Redox-sensitive polymeric nanoparticles for drug delivery*. Chemical Communications, 2012. **48**(48): p. 6043-6045.

18. Laurent, S., et al., *Magnetic iron oxide nanoparticles: synthesis, stabilization, vectorization, physicochemical characterizations, and biological applications*. Chemical reviews, 2008. **108**(6): p. 2064-2110.
19. Jang, J.t., et al., *Critical Enhancements of MRI Contrast and Hyperthermic Effects by Dopant-Controlled Magnetic Nanoparticles*. Angewandte Chemie, 2009. **121**(7): p. 1260-1264.
20. Figuerola, A., et al., *From iron oxide nanoparticles towards advanced iron-based inorganic materials designed for biomedical applications*. Pharmacological Research, 2010. **62**(2): p. 126-143.
21. Huber, D.L., *Synthesis, properties, and applications of iron nanoparticles*. Small, 2005. **1**(5): p. 482-501.
22. Skorvanek, I. and R.C. O'Handley, J. Magn. Mater., 1995. **140**: p. 467-469.
23. Ling, D. and T. Hyeon, *Chemical design of biocompatible iron oxide nanoparticles for medical applications*. Small, 2013. **9**(9-10): p. 1450-1466.
24. Massart, R., *Preparation of aqueous magnetic liquids in alkaline and acidic media*. IEEE transactions on magnetics, 1981: p. 1247-1248.
25. Jolivet, J.-P., É. Tronc, and C. Chanéac, *Synthesis of iron oxide-based magnetic nanomaterials and composites*. Comptes Rendus Chimie, 2002. **5**(10): p. 659-664.
26. Smolensky, E.D., et al., *Surface functionalization of magnetic iron oxide nanoparticles for MRI applications—effect of anchoring group and ligand exchange protocol*. Contrast media & molecular imaging, 2011. **6**(4): p. 189-199.
27. Kumfer, B.M., et al., *Gas-phase flame synthesis and properties of magnetic iron oxide nanoparticles with reduced oxidation state*. Journal of aerosol science, 2010. **41**(3): p. 257-265.
28. de Castro, V., et al., *Functionalisation of Glass with Iron Oxide Nanoparticles Produced by Laser Pyrolysis*. Journal of nanoscience and nanotechnology, 2008. **8**(5): p. 2458-2462.
29. Hyeon, T., et al., *Synthesis of highly crystalline and monodisperse maghemite nanocrystallites without a size-selection process*. Journal of the American Chemical Society, 2001. **123**(51): p. 12798-12801.
30. Thimmaiah, S., et al., *A solvothermal route to capped nanoparticles of  $\gamma$ -Fe<sub>2</sub>O<sub>3</sub> and CoFe<sub>2</sub>O<sub>4</sub>*. Journal of Materials Chemistry, 2001. **11**(12): p. 3215-3221.
31. Bronstein, L.M., et al., *Influence of iron oleate complex structure on iron oxide nanoparticle formation*. Chemistry of Materials, 2007. **19**(15): p. 3624-3632.
32. Gage, S.H., et al., *Functionalization of monodisperse iron oxide nps and their properties as magnetically recoverable catalysts*. Langmuir, 2012. **29**(1): p. 466-473.
33. Luigjes, B., et al., *Diverging geometric and magnetic size distributions of iron oxide nanocrystals*. The Journal of Physical Chemistry C, 2011. **115**(30): p. 14598-14605.
34. Park, J., et al., *Ultra-large-scale syntheses of monodisperse nanocrystals*. Nature materials, 2004. **3**(12): p. 891-895.

35. Teng, X. and H. Yang, *Effects of surfactants and synthetic conditions on the sizes and self-assembly of monodisperse iron oxide nanoparticles*. Journal of Materials Chemistry, 2004. **14**(4): p. 774-779.
36. Jana, N.R., Y. Chen, and X. Peng, *Size-and shape-controlled magnetic (Cr, Mn, Fe, Co, Ni) oxide nanocrystals via a simple and general approach*. Chemistry of materials, 2004. **16**(20): p. 3931-3935.
37. Huang, J.-H., et al., *Investigation of the growth mechanism of iron oxide nanoparticles via a seed-mediated method and its cytotoxicity studies*. The Journal of Physical Chemistry C, 2008. **112**(40): p. 15684-15690.
38. Kim, B.H., et al., *Large-scale synthesis of uniform and extremely small-sized iron oxide nanoparticles for high-resolution T 1 magnetic resonance imaging contrast agents*. Journal of the American Chemical Society, 2011. **133**(32): p. 12624-12631.
39. Ho, D., X. Sun, and S. Sun, *Monodisperse magnetic nanoparticles for theranostic applications*. Accounts of chemical research, 2011. **44**(10): p. 875-882.
40. Yoo, D., et al., *Theranostic magnetic nanoparticles*. Accounts of chemical research, 2011. **44**(10): p. 863-874.
41. Dilnawaz, F., et al., *Dual drug loaded superparamagnetic iron oxide nanoparticles for targeted cancer therapy*. Biomaterials, 2010. **31**(13): p. 3694-3706.
42. Nasongkla, N., et al., *Multifunctional polymeric micelles as cancer-targeted, MRI-ultrasensitive drug delivery systems*. Nano letters, 2006. **6**(11): p. 2427-2430.
43. Hwu, J.R., et al., *Targeted paclitaxel by conjugation to iron oxide and gold nanoparticles*. Journal of the American Chemical Society, 2008. **131**(1): p. 66-68.
44. Cheng, K., et al., *Porous hollow Fe<sub>3</sub>O<sub>4</sub> nanoparticles for targeted delivery and controlled release of cisplatin*. Journal of the American Chemical Society, 2009. **131**(30): p. 10637-10644.
45. Perez, J.M., et al., *Integrated nanosensors to determine levels and functional activity of human telomerase*. Neoplasia, 2008. **10**(10): p. 1066-1072.
46. Grimm, J., et al., *Novel nanosensors for rapid analysis of telomerase activity*. Cancer Research, 2004. **64**(2): p. 639-643.
47. El-Boubbou, K., et al., *Magnetic glyco-nanoparticles: a tool to detect, differentiate, and unlock the glyco-codes of cancer via magnetic resonance imaging*. Journal of the American Chemical Society, 2010. **132**(12): p. 4490-4499.
48. Colombo, M., et al., *Femtomolar detection of autoantibodies by magnetic relaxation nanosensors*. Analytical biochemistry, 2009. **392**(1): p. 96-102.
49. Brown, M.A. and R.C. Senelka, *MRI: Basic Principles and Applications*. Magnetic resonance imaging. 2010: Wiley-Blackwell & Co, New York. 661-674.
50. Lee, J.-H., et al., *Exchange-coupled magnetic nanoparticles for efficient heat induction*. Nature nanotechnology, 2011. **6**(7): p. 418-422.
51. Zhao, Q., et al., *Magnetic nanoparticle-based hyperthermia for head & neck cancer in mouse models*. Theranostics, 2012. **2**(1): p. 113.

52. Jordan, A., et al., *The effect of thermotherapy using magnetic nanoparticles on rat malignant glioma*. Journal of neuro-oncology, 2006. **78**(1): p. 7-14.
53. Douglas, F.J., et al., *Formation of octapod MnO nanoparticles with enhanced magnetic properties through kinetically-controlled thermal decomposition of polynuclear manganese complexes*. Nanoscale, 2014. **6**(1): p. 172-176.
54. Li, J., et al., *Understanding the metabolic fate and assessing the biosafety of MnO nanoparticles by metabolomic analysis*. Nanotechnology, 2013. **24**(45): p. 455102.
55. Na, H.B., et al., *Development of a T1 contrast agent for magnetic resonance imaging using MnO nanoparticles*. Angewandte Chemie, 2007. **119**(28): p. 5493-5497.
56. Huang, H., et al., *PEGylation of MnO nanoparticles via catechol–Mn chelation to improving T1-weighted magnetic resonance imaging application*. Journal of Applied Polymer Science, 2015. **132**(31).
57. Chevallier, P., et al., *Tailored biological retention and efficient clearance of pegylated ultra-small MnO nanoparticles as positive MRI contrast agents for molecular imaging*. Journal of Materials Chemistry B, 2014. **2**(13): p. 1779-1790.
58. Shin, J., et al., *Hollow manganese oxide nanoparticles as multifunctional agents for magnetic resonance imaging and drug delivery*. Angewandte Chemie International Edition, 2009. **48**(2): p. 321-324.
59. Huang, H., et al., *Fabrication and evaluation of tumor-targeted positive MRI contrast agent based on ultrasmall MnO nanoparticles*. Colloids and Surfaces B: Biointerfaces, 2015. **131**: p. 148-154.

# Chapter II

## CHAPTER II

## MAGNETIC RESONANCE IMAGING

Magnetic Resonance Imaging (MRI) is a technique of generating images used in medical field for diagnostic purposes, based on the physical principle of nuclear magnetic resonance. This technique exploits the magnetic properties of the nuclei with an odd mass number, such as protons, which have an unpaired spin. The spin is a fundamental property in nature (as charge and mass) and it is present in each elementary particle. It is identified by a multiple of  $\frac{1}{2}$  and can be positive (+) or negative (-). The spins tend to pair and in an atom with a pair number of elementary particles; they cancel each other.<sup>[1]</sup> Some substances have different orbital at the same energy level, which are filled with an electron at a time, all with parallel spin, creating paramagnetic materials (substances with unpaired electronic spins which possess magnetic properties). Each spin has an intrinsic angular momentum (vector often indicated by  $I$ ) which provides a magnetic moment ( $\mu$ ) generated by the rotation of the atomic nuclei on themselves. The magnetic moment is given by the equation:

$$\mu = \gamma I, \text{ eq. (2.1)}$$

where  $\gamma$  is the gyromagnetic ratio, a constant that for hydrogen it has the value of 46.2 MHz/T.<sup>[1]</sup> The spin can be seen as the rotation of a particle around its own axis and its precession around the axis of the magnetic field  $B_0$  (Fig. 2.1). In MRI the unpaired spin of the hydrogen proton (H) is used to generate images, mainly because of its abundance in the body, which are found for example in water ( $H_2O$ ) and in the fat ( $-CH_2$ ).

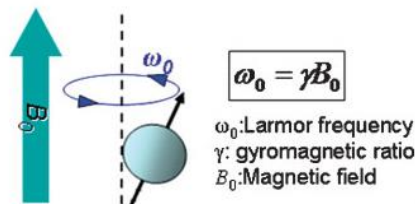


Fig. 2.1. Spins align parallel or antiparallel to the magnetic field and precessing as Larmor frequency ( $\omega_0$ ).<sup>[2]</sup>

When the nuclei of the protons are exposed to a strong magnetic field  $B_0$ , their spins are oriented either parallel or antiparallel to it. During their alignment, the spins precess under a specific frequency, known as the Larmor frequency ( $\omega_0$ ) that is defined by the equation of Larmor:



$$\omega_0 = \gamma \mathbf{B}_0, \text{ eq. (2.2)}$$

where  $\omega_0$  (Hz) is the resonance frequency of protons in a specific field and  $B_0$  [T] is the external magnetic field. This phenomenon is called proton precession.<sup>[1]</sup>

When the nuclei are subjected to a resonance frequency in the range of radio frequency (RF), the protons absorb energy and are excited to the antiparallel state. Eventually a small excess of spin will occupy the orientation along the magnetic field, since that's the state with lower energy. This will create a net magnetization,  $M$ , sum of all spins.<sup>[3]</sup> This net magnetization accumulates in a few seconds up to reach its maximum value (Fig. 2.2). The time it takes depends on the strength of  $B_0$  and the examined tissue type or, more specifically by the mobility of protons within the tissue. When the RF pulse stops, the excited nuclei relax and return to their equilibrium values.

There are two different relaxation pathways occurring at different speeds. The relaxation occurs along both the z-axis and the xy plane and are respectively called  $R_1$  ( $1/T_1$ ) and  $R_2$  ( $1/T_2$ ), where  $T_1$  or longitudinal relaxation time regards the increase of the net magnetization ( $M_z$ ) on the z-plane, while the  $T_2$  or transverse relaxation time, involves the decrease of the magnetization in the perpendicular plane  $M_{xy}$ .<sup>[2]</sup>

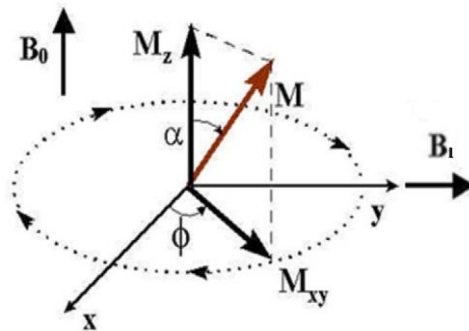


**Fig. 2.2.** Magnetization vectors during the RF pulse.  $\alpha$  will reach the maximum value while  $\phi$  different levels in the circle<sup>[3]</sup>.

When an RF pulse is applied to the spin, it generates a transverse magnetization in the xy plane ( $M_{xy}$ ) perpendicular to the direction of the static magnetic field. The net magnetization  $M$ , as a vector, has the components  $M_z$  and  $M_{xy}$  which produce the respective processes of spin (Fig. 2.3).

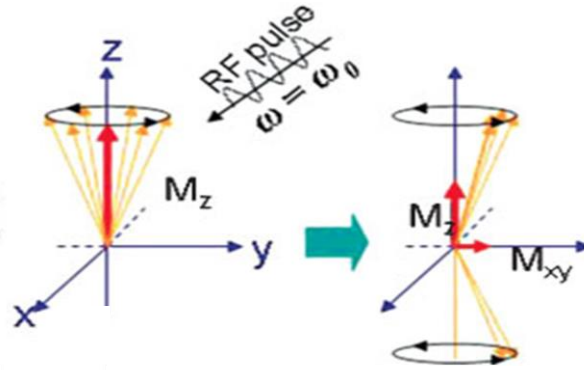


**Fig. 2.3.**Change of spin after the RF pulse <sup>[2]</sup>.

The change in  $M_z$  is due to energy transfer, while that in  $M_{xy}$  is due to the process of spin dephasing caused by the randomization of the magnetization of excited spins with the same phase coherence immediately after the application of the RF pulse.<sup>[2]</sup>

Inhomogeneities of the magnetic field can be present as the magnetic properties of an object can cause phase incoherence. The spin-spin interaction between the nuclei of hydrogen or electrons causes a loss of transverse coherence, which produces the real and characteristic relaxation time  $T_2$  of the tissues. Therefore, the transverse relaxation time is influenced by inhomogeneous magnetic fields produced from tissue-inherent factors or from external sources, and the total relaxation time  $T_2^*$ , is described by equation 2.3:

$$\frac{1}{T_2^*} = \frac{1}{T_2} + \gamma B_s, \text{ eq. (2.3)}$$

where  $\gamma B_s$  represents the relaxation caused by the inhomogeneities of the magnetic field and is called magnetic susceptibility.<sup>[2]</sup>

## 2.1 Relaxation times $T_1$ and $T_2$

The longitudinal relaxation time ( $T_1$ ) is characterized by the time it takes to re-align the spins along the Z axis ( $M_z$ ) after the RF pulse ceases and returns to approximately 63% of their equilibrium value  $M_0$  (Fig. 2.4.a) . It is defined by equation 2.4.

$$M_z(t) = M_0(1 - e^{-t/T_1}), \text{ eq. (2.4)}$$

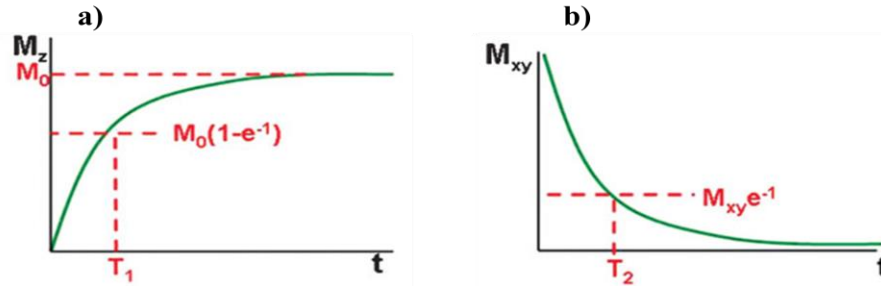


Fig. 2.4. a) Increased magnetization along the z axis. b) Decay of the magnetization in the xy plane.<sup>[2]</sup>

On the other hand, the transverse relaxation time ( $T_2$ ) is the time it takes the component of magnetization to decay in the plane  $M_{xy}$  (Fig. 2.4.b) and is described by the equation:

$$M_{xy}(t) = M_{xy}(0)(e^{-t/T_2}), \text{ eq. (2.5)}$$

Assuming that protons are exposed to the external static magnetic field  $B_0$ , after the RF pulse, the  $M_{xy}$  component returns to steady state and this depends only on the relaxation process. The phenomenon measured by a coil in the xy plane will cause the decay of the curve and can be compared to a sinusoidal curve (Fig. 2.5)



Fig. 2.5. Signal decay over time. <sup>[1]</sup>

Usually the relaxation time  $T_2$  is 5-10 times faster than the  $T_1$  due to the phase shift. The phase shift is the randomization of the magnetization vectors and the spins excited with the same phase coherence after the RF pulse. The phase shift occurs due to the inhomogeneity of the magnetic field  $\Delta B_z$  which are created by the magnet in the MR instrument or by internal inhomogeneities caused by the same spin. Since the spins can orient themselves with  $B_0$  or away from this, every spin influence its neighbor. Also the proton interactions with macromolecules, such as proteins or contrast agents in the tissue, can induce local changes of the magnetic field. Perturbations in the magnetic field will cause differences in the precession frequency of spin where  $B_0$  will be instead  $B_0 + \Delta B$ . The difference in frequency will cause an initial phase shift of the spins after the RF pulse. Since the net magnetization  $M_{xy}$  is the sum of all the vectors for all spins, when they begin to go out of phase, the sum of the vectors decreases rapidly. <sup>[1]</sup>

$T_2$  depends on how fast protons in tissue lose their phase coherence and it is associated with their density. High density means more spin-spin interactions and faster phase shift (Table 2.1). Fluids for example have relatively long distances between molecules and therefore long  $T_2$ .

**Table.2.1:**  $T_1$  and  $T_2$  properties for three different types of tissues. <sup>[1]</sup>

	Fluids	Solids	Fat and Protein rich tissue
$T_1$	Non efficient energy transfer	Inefficient energy transfer	Efficient energy transfer
	Very long $T_1$	Long $T_1$	Short $T_1$
$T_2$	Less dephasing	Most dephasing	Intermediate dephasing
	Long $T_2$	Short $T_2$	Intermediate $T_2$

The characteristics  $T_1$  in a tissue have to do with the efficiency of proton transfer. Experimental data have shown that the transfer of the proton energy will be more efficient when the vibration/rotation frequencies of the molecules are similar to those of Larmor.

As shown before, the Larmor frequency depends on the magnetic field (eq. 2.2), while the vibrational frequencies depend on the physical state of the tissue. Water vibrations cause fluctuations of the protons at the same frequency of the magnetic field and this disturbance in the magnetic field stimulates the relaxation. The natural rotational frequency for fat between the natural C-C bonds is close to the Larmor frequency and therefore has efficient transfer of energy. The opposite occurs for small water molecules that vibrate at much higher frequency leading to a lower energy transfer (Tab. 2.2)

**Table.2. 2:** Approximate values of  $T_1$  and  $T_2$  in humans. <sup>[1]</sup>

Tissue type	Approximate $T_1$ [ms]	Approximate $T_2$ [ms]	Main field [T]
Adipose tissues	240-250	60-80	1.5
Whole blood (oxygenated)	1350	200	1.5
Cerebrospinal fluid	2200-2400	500-1400	1.5
Grey matter	920	100	1.5
White matter	780	90	1.5
Liver	490	40	1.5
Kidneys	650	60-75	1.5
Muscle	860-900	50	1.5

### 2.1.1. $T_1$ -weighted images and Repetition Time (TR)

To be able to create a  $T_1$ -weighted image, the site of interest must be excited several times. The time between two consecutive RF pulses is defined as Repetition Time (TR) and it directly affects the  $T_1$  contrast due to it regulates the amount of time available for relaxation after the pulse. A long TR allows a better realignment along the z axis and a bigger angle to overturn a radio frequency. Choosing a short TR will highlight tissues with short  $T_1$ , which will be able to recover at a higher level. This will give a bigger net magnetization which gives a brighter spot to the image. On the other side, tissues with longer  $T_1$  will not have much time to relax and consequently they will have a smaller net magnetization. This type of image with short TR contains more information about  $T_1$  and is therefore called  $T_1$ -weighted.<sup>[1]</sup>

### 2.1.2. $T_2$ -weighted images and echo time (TE)

The echo time (TE) is the time between the RF pulse and the measurement and it has a direct influence on the  $T_2$  contrast. By choosing a TE of the same order of magnitude of the  $T_2$  of the tissue, it will underline differences in the relaxivity. Tissues with short  $T_2$  will be more phase shifted and they will lose much of their net magnetization  $M_{xy}$ , while tissues with long  $T_2$  will still have a strong signal. Since a short  $T_2$  will give a faster phase shift and a faster signal loss, tissues with short  $T_2$  will appear darker. The greater the difference between the decay curves, the result will be a sharp and clear contrast (Fig. 2.6). For this reason,  $T_2$  contrast agents are designed in order to increase these differences. Images acquired with a long TR and a long TE will give a dark spot for tissues with short  $T_2$  (Tab. 2.2) and are called  $T_2$ -weighted images.

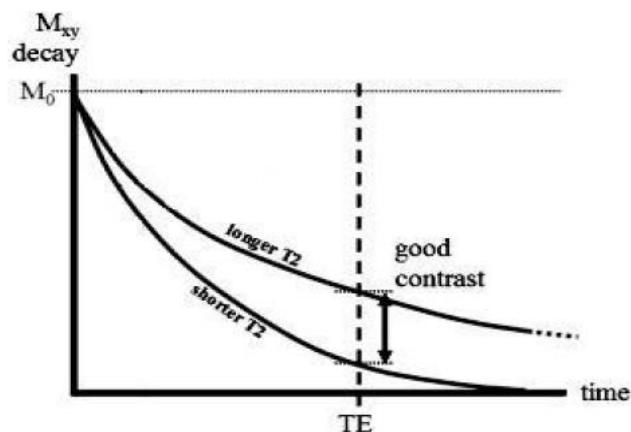


Fig.2.6. Differences between decay curves lead to a sharper contrast.<sup>[1]</sup>

### 2.1.3 Magnetic Susceptibility

All materials acquire a certain degree of magnetization when subjected to a magnetic field. The magnetic susceptibility is a measure of how much a material can be magnetized and is defined by  $M = \chi H$  where  $M$  is the magnetization and  $H$  [A/m] the field.

Ferromagnetic materials, normally magnets, are permanently magnetized because of their small magnetic domain where all the magnetic moments are aligned. The domains themselves are randomly oriented one to another causing a cancellation of the magnetization of the entire material. When the latter is subjected to an external magnetic field, the domains align with this and the material becomes permanently magnetized.

Paramagnetic substances instead become magnetized when an external magnetic field is applied but they lose their magnetization when the magnetic field is interrupted. Materials with a large number of unpaired spin, for example gadolinium with seven unpaired electrons, are highly paramagnetic. Following the external magnetic field, the magnetic moments of these unpaired spin create a net magnetization when oriented (Fig 2.7).

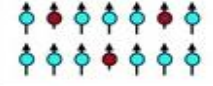
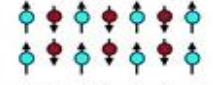


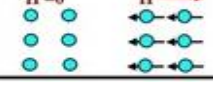
type	spin alignment	spin in simplified plot	examples
ferromagnetic	all spins align parallel to one another: spontaneous magnetization- $M = a + b$		Fe, Co, Ni, Gd, Dy, SmCo <sub>5</sub> , Sm <sub>2</sub> Co <sub>17</sub> , Nd <sub>2</sub> Fe <sub>14</sub> B
ferrimagnetic	most spins parallel to one another, some spins antiparallel: spontaneous magnetization- $M = a - b > 0$		magnetite (Fe <sub>3</sub> O <sub>4</sub> ), yttrium iron garnet (YIG), GdCo <sub>5</sub>
antiferromagnetic	periodic parallel-antiparallel spin distribution: $M = a - b = 0$		chromium, FeMn, NiO
paramagnetic	spins tend to align parallel to an external magnetic field: $M = 0 @ H=0, M > 0 @ H > 0$		oxygen, sodium, aluminum, calcium, uranium
diamagnetic	spins tend to align antiparallel to an external magnetic field: $M = 0 @ H=0, M < 0 @ H > 0$		superconductors, nitrogen, copper, silver, gold, water, organic compounds

Fig. 2.7: Magnetic Behaviors (Magnet Energy Corporation ®)

In the other hand, superparamagnetism occurs when the material is composed of very small crystal domains, for example in a single nanoparticle with a hydrodynamic diameter,  $D_h < 30\text{nm}$ . In this case, when the temperature is close to the temperature of Curie or Neel (thermal energy needed to overcome the coupling forces between neighboring atoms and destroy any magnetic order, transforming the paramagnetic material) the thermal energy is sufficient to change the direction of magnetization of the entire crystal.<sup>[3]</sup>

The resulting rapid fluctuations in the direction of the magnetization lead to a zero mean, therefore, the material behaves similar to a paramagnetic, with the exception that there are no changes at the level of each individual atom but the direction around the crystal changes. Under the influence of an external magnetic field, the magnetic moment of the entire crystal will align with this by giving the material a susceptibility from 100 to 1000 times stronger.

## **2.2. MRI contrast agents based on magnetic nanoparticles**

Among the currently existing imaging techniques such as x-ray, ultrasound, radioactive markers; MRI is the most used diagnostic tool since compared to the other it has the following advantages:

- Non-invasive
- Production of images with high spatial resolution that allow discriminating tissues according to their biochemical composition.
- Safety for the patient since it is not subjected to ionizing radiation or radioactive isotopes

However, the main limitations are:

- Costs and time required for image acquisition
- Difficulties in the differentiation of tissues magnetically similar but histologically different (healthy tissue from diseased tissue).

These limitations can be overcome by the use of contrast agents which shorten the relaxation times of the spins of the water molecules of the desired tissue and increase the contrast with the surrounding tissues, thus obtaining high-quality images.

Most of the contrast agents commercially available are constituted by paramagnetic complexes. Their first clinical applications were directed to identify the breakage of the blood brain barrier (BBB), changes in the vasculature, flow changes and perfusion. Recently, several studies have been carried out in order to develop new contrast agents for MRI based on magnetic nanoparticles, which are composed by a magnetic and its appropriate surface coating.

In the last twenty years the focus has shifted to a new class of contrast agents, consisting of superparamagnetic iron oxide (SPIO), used primarily as a contrast to the liver. This was the first nanostructured contrast agent currently still in use in the clinic.

Nanostructured contrast agents for MRI are formed from three parts (Fig 2.8):

- 1) The nanoparticle core which generates the signal increase.
- 2) The shell, which makes the nanoparticle dispersible in water and thus stable in a biological environment.
- 3) The bioactive material required for a specific targeting.

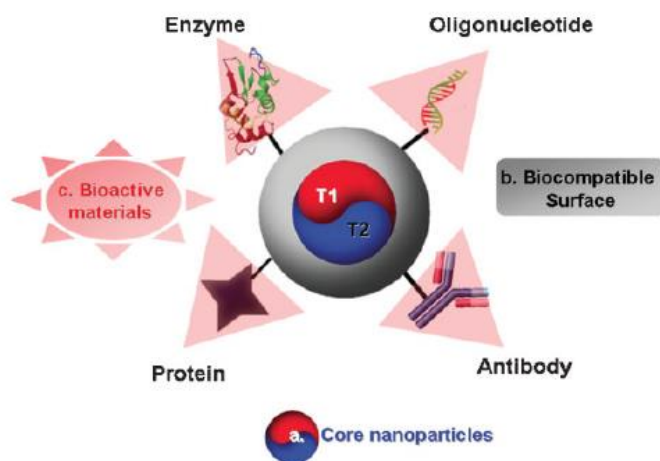


Fig. 2.8: Structure of a nanostructured contrast agent.<sup>[2]</sup>

### 2.2.1 Surface biocompatibility

For many biomedical applications, in particular for *in vivo* imaging, nanoparticles should have good colloidal stability and low toxicity in a biological environment. Although there have been synthesized magnetic nanoparticles of high quality with uniform size and high crystallinity by thermal decomposition of metal precursors in organic media, these are hydrophobic, and consequently are not stable in an aqueous environment for biomedical applications.<sup>[4]</sup> Surface modification of these nanoparticles is essential to give them hydrophilic properties so that they can be widely used for various biomedical applications. In addition, surface modification is required to increase the functions of the nanoparticle since it is possible to conjugate bioactive material through reactive groups exposed on the surface.

Between the different methods of surface modification currently existing, the more representative strategies are:

- Ligand exchange: allows incorporating water dispersible ligands and encapsulation with biocompatible shells.



Nanoparticles in organic solvents are stabilized by surfactants that have their hydrophilic groups bound to the surface of the nanoparticles and the hydrophobic hydrocarbon tails toward the solvent. Since the atoms on the nanoparticles surface have affinity towards the functional groups, surface functionalization with suitable hydrophilic binders allows the phase transfer of the nanoparticles from organic solvent to aqueous media.

This ligand-exchange method has several advantages such as the simple procedure, passivating thin layer and overall small size. Metal oxide nanoparticles have little reactive surfaces when compared to other types of nanoparticles as there are a limited number of functional groups available. This has prompted research towards strong ligand systems in particular for iron oxide nanoparticles. For example, dopamine has been used as a binder to immobilize functional molecules in iron oxide nanoparticles, while Peng and co-workers have taken advantage of the interactions between hydroxamic acid and iron oxide.<sup>[5]</sup> Cheon and co-workers have been able to synthesize water-dispersible iron oxide nanoparticles using 2,3-dimercaptosuccinic acid (DMSA), which has a bidentate carboxyl group.<sup>[6]</sup> The resulting iron oxide nanoparticles are water dispersible and have been successfully used for MRI. To improve nanoparticles biocompatibility, the ligands skeleton is designed to contain biocompatible polymers, such as poly (ethylene glycol) (PEG). Ligands of derivatized phosphine oxide with PEG (PEG-PO) consist of a biocompatible tail of PEG, and a phosphine oxide head coordinated on the nanoparticles surface allowing stabilizing different types of nanoparticles in aqueous media.<sup>[7]</sup> Polymeric ligands or dendrimers have also been used for the stabilization of iron oxide nanoparticles in aqueous media resulting from their multiple functional groups and bulky structures.

- The second strategy of surface modification is the formation of a biocompatible shell around the nanoparticles. There are a variety of biocompatible methods for making the shell, which can be classified according to the materials used and their encapsulation processes. The most used materials are silica and polymer. Crosslinked shells of amorphous silica can stabilize nanoparticles. Although the toxicity of the silica in nanometric dimensions is still in debate, there have been promising reports in vitro and in vivo regarding silica coated nanoparticles. For example, Ying and collaborators have reported silica coated nanoparticles produced by a base-catalyzed reaction with formation of silica via inverse microemulsion.<sup>[8]</sup> Although the silica layer is relatively thick (10-30 nm), the encapsulation process is simple and it is possible to encapsulate multiple or different nanoparticles within the shell.

---

Silica shells have a charge of their own and are sensitive to the pH of the surrounding medium, which can cause precipitation and gel formation. For that reason, additional biocompatible polymers have been linked on the silica shell surface to improve their colloidal stability.<sup>[8]</sup>

The immobilization of magnetic nanoparticles with polymers clinically used can reduce problems regarding safety and toxicity. These hybrid-polymer nanoparticles can be used for multifunctional applications such as drug delivery and imaging. Polyesters, such as poly (D, L-lactic-co-glycolic acid) (PLGA), poly (D, L-lactic acid) (PLA) and poly (glycol acid) (PGA), have been the most commonly used for these applications. In particular, poly (Ethylene Glycol) (PEG), a biocompatible polymer, has received great attention due to its nonfouling structure and its ability to bypass the (reticuloendothelial system) RES and natural barriers, such as the nasal mucosa. PEG has been widely used as a stabilizer for many nanoparticles used in biomedical applications, particularly in long circulation imaging systems *in vivo*. Since PEG is inert itself, it is possible to anchor on its surface materials such as copolymers, phospholipids, and silica, to encapsulate the nanoparticles. Dubertret et al. have reported that block copolymers of PEG-phospholipids may form a stable micelle structure on quantum dots via the hydrophobic interaction between the hydrophobic groups of the surfactant tail and the phospholipid parts.<sup>[9]</sup> In this way, the outer surface of the nanoparticles is composed of a dense layer of PEG, which is stable in the biological medium. This process is very reliable, and can be generally applicable to many other types of nanoparticles. Using a similar strategy, various water dispersible metal oxides nanoparticles, including iron oxide, have been generated. However, since these block copolymers PEG-phospholipids are very expensive, they cannot be prepared on a large scale.

To make water soluble nanoparticles, di/tri-blocks of amphiphilic copolymers have also been used. Their hydrophobic blocks may interact with the hydrophobic surface of the nanoparticles, while the outer hydrophilic block makes nanoparticles dispersible in water. These block copolymers are relatively inexpensive, and can be modified with other functional groups for further functionalization. However, the disadvantage of using these block polymers is the great thickness of the shell due to their high molecular weight, which limits many of their applications.

Oligomeric and dendritic molecules have also been used as materials for nanoparticles coating making them water-dispersible because they form thinner shells while maintaining its stability in aqueous solution.

For example, Yang and coworkers have shown that cyclic oligosaccharides, which have hydrophobic cavities and hydrophilic rings, allow nanoparticles transfer from an organic phase to aqueous media.<sup>[10]</sup> At the same time, Weller and colleagues have shown that the relaxivity of magnetic nanoparticles depends not only on the size of the core of the nanoparticles, but also on the type of shell.<sup>[11]</sup>  $\text{MnFe}_2\text{O}_4$  nanoparticles synthesized in ether were transferred into water using three different approaches, namely ligand-exchange to form a water soluble polymer shell, embedding in an amphiphilic polymer shell, and encapsulation in large micelles formed by lipids. In the first two systems based on polymers, nanoparticles were individually and homogeneously dispersed with hydrodynamic radius of 30-40 nm, while the aggregated nanoparticles were randomly distributed inside the micelles with hydrodynamic radius of 250 nm. It is noteworthy that the relaxivity  $r_2^*$  is much higher for the micellar system than for particles stabilized by the polymer using nanoparticles of the same size (Fig. 2.9).

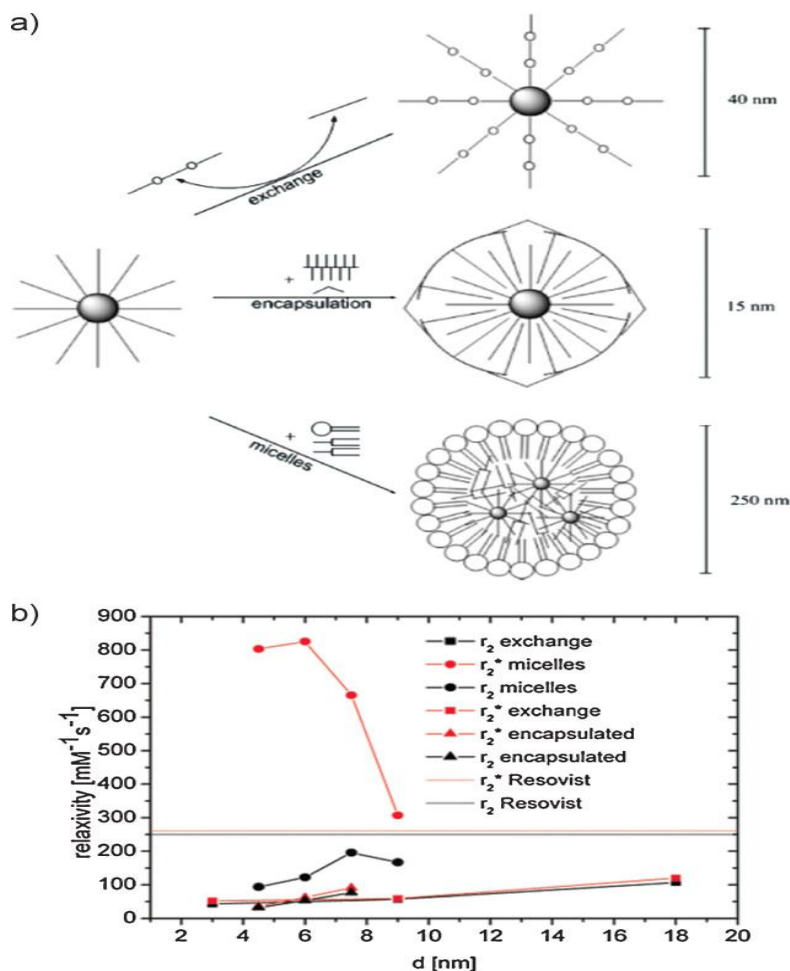


**Fig. 2.9:** a) Three methods of preparation of water dispersible manganese ferrite nanoparticles b)  $r_2$  relaxivity values of manganese ferrite nanoparticles with three types of coating.<sup>[11]</sup>

### 2.3. T<sub>2</sub> contrast agents

T<sub>2</sub> contrast agents commercially available are based on iron oxide nanoparticles, Fe<sub>3</sub>O<sub>4</sub>, which have paramagnetic properties with a much larger magnetic susceptibility compared to paramagnetic materials. Iron oxide is ferromagnetic in its single form and has a large magnetic susceptibility that persists even without applying an external magnetic field. In the nanoscale, iron oxide particles lose their ability to maintain the magnetization without an external field thus becoming superparamagnetic. When a magnetic field is applied they exhibit a strong magnetization that causes inhomogeneity of the field. These disturbances affect the precession frequency of several spin making them slightly different. Superparamagnetic substances cause severe disturbances which lead to big differences in the precession frequency and therefore a faster phase shift. Since T<sub>2</sub> agents produce an effective decrease of the signal, they are called negative contrast agents and they must have an R<sub>2</sub> value as large as possible for it to be effective. This effect of signal decrement is the main disadvantage of T<sub>2</sub> contrast agents as it means that particular details are lost.<sup>[2]</sup> The dark area can be confused with other pathogenic conditions, such as bleeding or metal deposition, or with organs such as the lungs which are dark due to the low proton density in the air. The advantage of these contrast agents is given by the nanoparticles size which is the main factor controlling characteristics such as the half-life in blood and their distribution. Small particles (DH <20nm) can penetrate easily through the blood vessels walls, tissues and the lymphatic system allowing thus intracellular imaging and stem cells tracking.

Iron oxide nanoparticles (magnetite Fe<sub>3</sub>O<sub>4</sub> or maghemite  $\gamma$ -Fe<sub>2</sub>O<sub>3</sub>) have been successfully used thanks to their ability to shorten the T<sub>2</sub> relaxation time in the liver, spleen and bone marrow with a selective uptake and accumulation in cells of the reticuloendothelial system (RES). Their biological distribution depends predominantly on their size and they can be classified into: 1) paramagnetic iron oxide nanoparticles of micrometric size (MPIO; some micrometers), 2) superparamagnetic iron oxide (SPIO; a hundred nanometers) and 3) ultra small superparamagnetic iron oxide (USPIO; less than 50 nm). The most representative methods for preparing SPIOs and USPIOs involve coprecipitation reactions of a mixture of ferrous and ferric salts in aqueous medium in the presence of stabilizers such as hydrophilic polymers. This process is adopted for the synthesis of different contrast agents based in iron oxide nanoparticles currently in use such as Feridex®, Resovist®, and Combidex®.

These particles are formed by multiple core of iron oxide stabilized by a dextran based shell. Some of their physicochemical properties are shown in Table 2.3.

**Table.2.3:** Properties of T<sub>2</sub> contrast agents based on Iron.<sup>[2]</sup>

Name	Core Material	Surface	Diameter of Core [nm]	Hydrodynamic Diameter [nm]	Magnetization [emu g <sup>-1</sup> ][a]	r <sub>2</sub> [mM <sup>-1</sup> s <sup>-1</sup> ]	B <sub>0</sub> [T]
Ferumoxides (Feridex)	Fe <sub>3</sub> O <sub>4</sub> , γ-Fe <sub>2</sub> O <sub>3</sub>	Dextran	4.96	160	45	120	1.5
Ferucarbotran (Resovist)	Fe <sub>3</sub> O <sub>4</sub>	Carboxydextran	4	60		186	1.5
Ferumoxtran (Combidex)	Fe <sub>3</sub> O <sub>4</sub>	Dextran	5.85	35	61	65	1.5
CLIO-Tat	Fe <sub>3</sub> O <sub>4</sub>	Dextran	5	30	60	62	1.5
WSIO (MEIO)	Fe <sub>3</sub> O <sub>4</sub>	DMSA[b]	4		25	78	1.5
			6		43	106	
			9		80	130	
			12		101	218	
FeNP	α-Fe	PEG	10		70	129	1.5
MnMEIO	MnFe <sub>2</sub> O <sub>4</sub>	DMSA[b]	6		68	208	1.5
			9		98	265	
			12		110	358	
CoMEIO	CoFe <sub>2</sub> O <sub>4</sub>	DMSA[b]	12		99	172	1.5
NiMEIO	NiFe <sub>2</sub> O <sub>4</sub>	DMSA[b]	12		85	152	1.5
Au-Fe <sub>3</sub> O <sub>4</sub>	Fe <sub>3</sub> O <sub>4</sub>	PEG	20			114	3.0
Au-FePt	FePt (fcc)	PEG	6			59	3.0

[a] Magnetic properties were measured at 1.5 T external field. [b] 2,3-Dimercaptosuccinic acid.

The main target of SPIO at the clinical level is hepatic system as the SPIO are taken by the Kupffer cells in the liver, spleen, and bone marrow. When it is affected by liver diseases such as primary tumor or metastases, these regions will have a shortage of Kupffer cells, causing a negligible uptake of the SPIO in diseased tissue, thus allowing obtaining a high contrast between normal and diseased tissues.

Since small nanoparticles have longer circulation time in plasma because of their low excretion by the liver, iron oxide nanoparticles required for molecular imaging are usually in the class USPIO (<50 nm). A typical clinical application of USPIOs is the imaging of lymph nodes. The detection of lymph nodes is crucial to evaluate the stage of the tumor and to plan a subsequent treatment. Extravasation of USPIOs from the interstitial spaces in the blood vessels allows their transport to the lymph nodes through the lymphatic vessels. Since the phagocytic activity by macrophages in lymph nodes with tumor cells is absent, injected nanoparticles will remain only in normal lymph nodes and their accumulation will allow sensitive differentiation between normal and malignant cells (Fig. 2.10 a).

Regarding this application, Weissleder and collaborators reported the successful detection of lymph node metastases in patients with prostate cancer using USPIO.<sup>[12]</sup> The USPIOs were tested as blood pool agents due to they were readily distributed in the extracellular space.

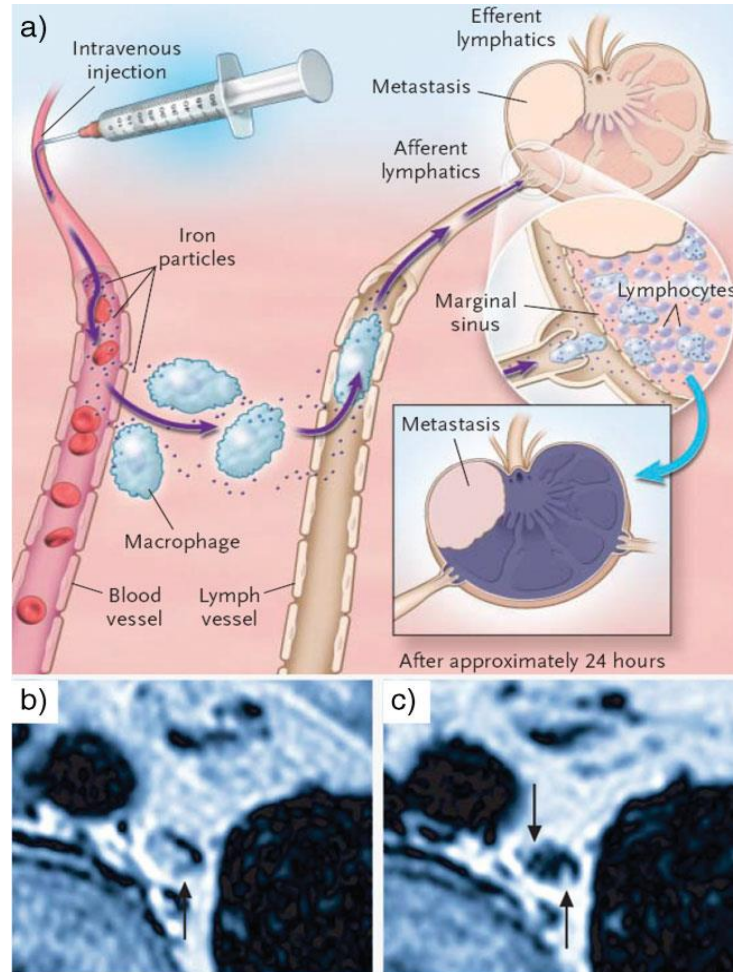


**Fig. 2.10:** a) Mechanism of action of USPIO. b, c) MR images of a metastatic lymph node b) before and c) after USPIO.<sup>[12]</sup>

Cell therapy is a personalized treatment that has been used for more than 50 years. In particular, recent research on stem cells gives hope to people suffering incurable diseases. Monitoring noninvasively differentiation and distribution of the cells *in vivo* can develop a successful cell therapy. *In vivo* MRI has been performed with cells labeled with SPIO and USPIO *ex vivo* using neutrophils, macrophages and monocytes, as cells with phagocytic activity while lymphocytes and stem cells were used as cells with phagocytic activity lacking. In early studies, cells were labeled by simple incubation with a high concentration of nanoparticles.

The long incubation time required and the low efficiency in chemically marking the non-phagocytic cells has prompted research into biological approaches. For that reason, electroporation methods and the use of transfection agents have been adapted of for introducing DNA or plasmids. Bulte et al. have efficiently marked stem cells with magnetic iron oxide through electromagnetoporation, combining the variations of the electromechanical permeability of the cell membrane and the accelerated movements of iron oxide in a magnetic field.<sup>[2]</sup>

Another approach is the functionalization of the nanoparticles with materials that facilitate the binding on the anionic cell membrane, thus allowing its internalization into the cell. Viruses, peptides, proteins and antibodies have been conjugated to SPIO and USPIO. In particular, monocrystalline iron oxide nanoparticles (MION) stabilized with dextran have been conjugated with biomaterials due to the fact that they can be easily functionalized with amine groups by treatment with epichlorohydrin. Josephson et al. have reported that iron oxide nanoparticles conjugated with HIV-Tat (Tat-CLIO) proteins allow an effective marking of non-phagocytic cells activated by macropinocytosis.<sup>[13]</sup> The process of functionalizing dextran stabilized iron oxide nanoparticles via amino groups (crosslinked iron oxide, CLIO) has established an active platform of molecular imaging. Many types of biomolecules, including antibodies, proteins, peptides, polysaccharides and aptamers, have been covalently bonded on the surface of iron oxide nanoparticles for their specific accumulation at the site of interest. Furthermore, the amino groups may be conjugated with small molecules, such as dyes for multimode imaging and synthetic binders for the development of targeted images. Weissleder and colleagues developed biocompatible magnetic relaxation switches (MRS) to detect molecular interactions, such as DNA-DNA, protein-protein, protein-small molecule, and enzymatic reactions.<sup>[12]</sup> Results shown that self-assembling magnetic nanoparticles have spin-spin relaxation times ( $T_2$ ) bigger compared to the dispersions of individual nanoparticles.

### **2.3.1. Nanostructured $T_2$ contrast agents with improved magnetic properties**

The acceleration of the spin-spin relaxation time ( $T_2$  shortening) by magnetic nanoparticles is the result of the phase shift of the magnetic moments due to magnetic field gradients created by the small magnetized particles. In this process, the main mechanism of relaxation is the dipolar interaction between the spins of the water protons and the magnetic moment of the nanoparticles.

Therefore, as shown in the model suggested by Koenig and Keller, the spin-spin relaxation depends on the magnetic moment of the nanoparticles ( $\mu$ ) and is described by equation 2.6:

$$R_2 = \frac{1}{T_2} = \frac{a}{d_{NP}} D \gamma^2 \mu^2 C_{NP} J(\omega, \tau_D), \text{ eq. (2.6)}$$

where  $a$  is a constant;  $d_{NP}$  the nanoparticle diameter;  $D$  the diffusion coefficient;  $\mu$  the magnetic moment of the nanoparticle;  $\gamma$  the gyromagnetic ratio of the water protons;  $C_{NP}$  nanoparticles concentration; and  $J(\omega, \tau_D)$  the density spectral function.<sup>[1]</sup>

To be an effective  $T_2$  contrast agent, nanoparticles should have a large magnetization. Although magnetism is an intrinsic property of materials (bulk material), the magnetic properties of the nanoparticles are strongly dependent on their size, shape, and surface properties. A dramatic increase in surface area, induces a surface-canting effect, and consequently increases the net magnetization which is described by equation 2.7:

$$m_s = M_s \left[ \frac{(r-d)}{r} \right]^3, \text{ eq. (2.7)}$$

where  $m_s$  is the saturation magnetization of the nanoparticle,  $M_s$  the saturation magnetization of the bulk material,  $r$  the size of the nanoparticle, and  $d$  the thickness of the surface layer.<sup>[1]</sup>

For the production of efficient  $T_2$  contrast media it is necessary to control the magnetic properties of the nanoparticles through a precise design of the intrinsic properties of the material, such as composition and crystalline structure of the material, and extrinsic factors, such as size and shape. As mentioned before, most of the  $T_2$  contrast media are composed of aggregated nanoparticles with a multiple iron oxide core (4-5 nm) and dextran coatings. In the last decade monodisperse and highly crystalline iron oxide nanoparticles have been synthesized with various synthetic methods. The most representative is the thermal decomposition of metal precursors in a solution with organic surfactant at high temperature  $> 300$  °C (Fig. 2.11). In particular, Hyeon et al. have reported large scale production of different metal oxide nanoparticles, including iron oxide, by thermal decomposition of metal-surfactant complexes that were generated starting from inexpensive and non-toxic metal salts.<sup>[7]</sup> Iron oxide nanoparticles of small size have a large magnetization and a high relaxivity  $r_2$  which makes possible the increase of the sensitivity of  $T_2$ -weighted images and the reduction of their toxicity by decreasing the doses.



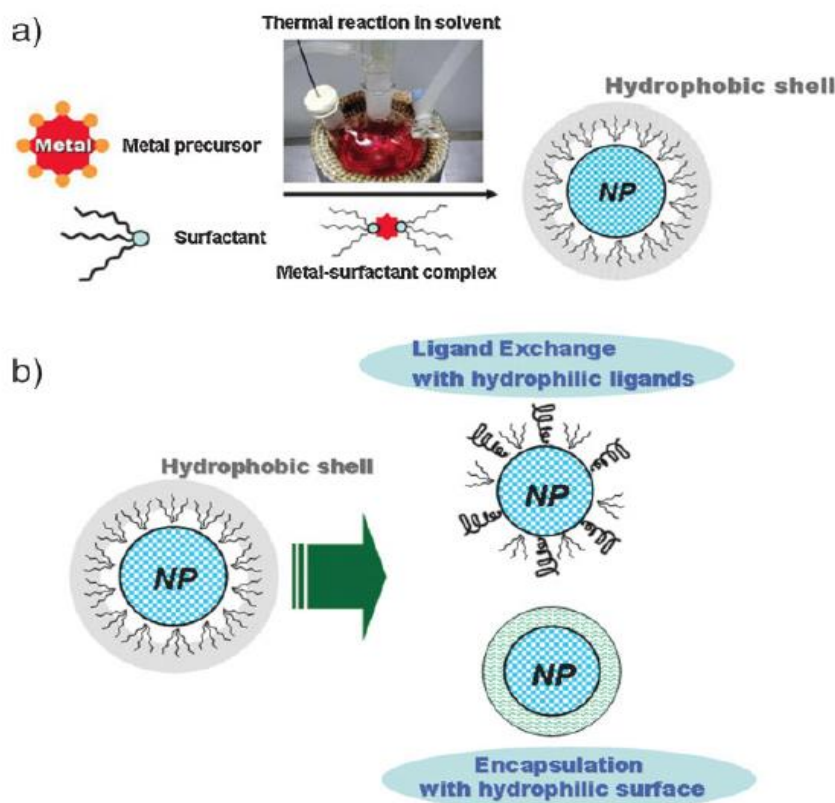


**Fig. 2.11:** a) Reaction scheme for the synthesis of monodispersed nanoparticles via thermal decomposition. b) Surface modification of hydrophobic nanoparticle.<sup>[2]</sup>

### 2.3.2. Multifunctional T<sub>2</sub> contrast agents

Water dispersible iron oxide nanoparticles have been widely used to the diagnosis of tumors. They can spontaneously accumulate in malicious sites thanks to the enhanced permeability and retention effect (EPR), which allows an increase of the accumulation of macromolecular species, including nanoparticles, in tumor tissues that have abnormal blood vessels. For a more efficient analysis, the surfaces of the iron oxide nanoparticles can be conjugated with targeting sensors, such as antibodies and proteins. For example, Cheon and co-workers have prepared iron oxide nanoparticles conjugated with Herceptin thus allowing the identification of tumor cells through interaction with the receptor of the human epidermal growth factor (Her2/neu), which is usually overexpressed in breast cancers.<sup>[14]</sup> At the same time, Gao and colleagues have conjugated a monoclonal antibody for targeting cancer (anti-carcinoembryonic antigen (CEA)) to iron oxide nanoparticles uniformly coated with PEG, and have successfully performed magnetic resonance of the human colon carcinoma.<sup>[14]</sup>

On the other hand, manganese ferrite nanoparticles conjugated with Herceptin (MnMEIO) have shown a highly efficient target in *in vivo* imaging of mice in order to detect very small tumors (Fig. 2.12). This result shows that advanced contrast agents consisting of nanoparticles with high magnetic moment and with appropriate targeting, could allow the ultrasensitive detection of various types of cancer by T<sub>2</sub>-weighted MR images. In this way, new nanomedical multifunctional platforms have been manufactured through the combination of different nanostructured materials with different functions, making possible the simultaneous realization of imaging, diagnosis and therapy.

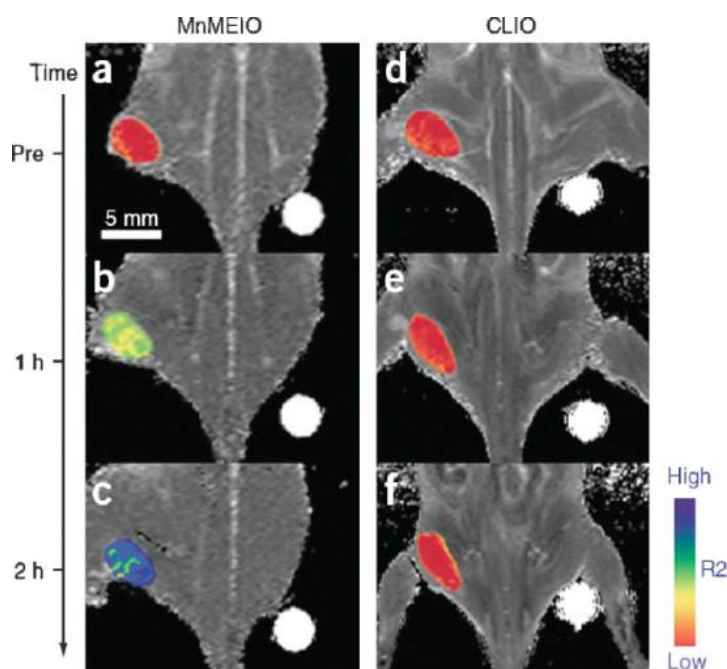


**Fig. 2.12:** MR images *in vivo* after administration of magnetic nanoparticles conjugated with Herceptin. a-c) Manganese ferrite nanoparticles (MnMEIO) show an increase in the signal higher than those with crosslinked iron oxide (CLIO) d-f).<sup>[14]</sup>

### Toxicity of Iron oxide

Iron oxide is considered safe due to the large metabolic activity involving the iron, where iron oxide is metabolized to elemental iron by the hydrolytic enzymes or under acidic conditions such as the interior of lysosomes. However clinical trials to evaluate the side effects of iron based nanostructured contrast agents, specifically Feridex®, showed a high incidence of side effects with 7.4% of patients (114/1535 subjects) reporting back pain and legs. In addition, 2.6% of patients showed such an intense pain to cause interruption of the infusion.

The largest clinical study was conducted in 1995 and involved 208 patients in the phase III trial. Patients received 213 doses of 10  $\mu\text{mol Fe/kg}$ . Although eight percent showed adverse reactions related to the administration of the drug, very severe conditions were not reported.<sup>[3]</sup>

### **Disadvantages of T<sub>2</sub> contrast agents**

Over the past twenty years iron oxide nanoparticles have been used as T<sub>2</sub> contrast agents for MRI. However there are some drawbacks that limit their application at the clinical level.

- Since they are negative contrast agents they produce a decrease of the signal. The resulting dark signal could be confused with other pathogenic conditions, bleeding, calcification or metal deposits.
- Their high sensitivity causes distortion of the magnetic field of the nearby normal tissues, known as artifact susceptibility or blooming effect, thus generating dark images and demolishing the background around the injury.

For these reasons, in recent years, it has been an increased interest on the development of new positive contrast agents, also called as T<sub>1</sub> contrast agents.<sup>[3]</sup>

### **2.4. T<sub>1</sub> contrast agents**

T<sub>1</sub> relaxation is the process of rebalancing the net magnetization (M<sub>z</sub>) after applying an RF pulse. This change of M<sub>z</sub> is a consequence of the energy transfer between the protons spins system and the surrounded molecules matrix. All biological systems are composed of various molecules thus showing different relaxation patterns and different T<sub>1</sub> relaxation times. The presence of paramagnetic ions in the vicinity of the tissue enhances relaxation and shortens the T<sub>1</sub> relaxation time. In particular, transition metals and lanthanides with a large number of unpaired electrons, such as Gd<sup>3+</sup>, Mn<sup>2+</sup>, and Fe<sup>3+</sup>, show very effective relaxation (Table 2.4). Since they are paramagnetic, T<sub>1</sub> contrast agents do not interrupt the magnetic homogeneity on large dimensions and therefore do not disturb the anatomical backgrounds. Moreover, these contrast agents should meet the following characteristics: 1) positive contrast capacity (T<sub>1</sub>), 2) easy absorption and intracellular accumulation for cell imaging, 3) adequate nanoparticle shape for easy surface modification and for binding bioactive materials, and 4) a favorable pharmacokinetics and an adequate dynamic for their efficient distribution towards biomarkers with minimal side effects.

**Table 2.4:** Electronic configuration and magnetic moment of metal ions.<sup>[3]</sup>

	Ion	Configuration		Magnetic moment
		3d	4f	
Transition metal ion	<sup>24</sup> Cr <sup>3+</sup>	↑ ↑ ↑ — —		3.88
	<sup>25</sup> Mn <sup>2+</sup>	↑ ↑ ↑ ↑ ↑		5.92
	<sup>26</sup> Fe <sup>3+</sup>	↑ ↑ ↑ ↑ ↑		5.92
	<sup>29</sup> Cu <sup>2+</sup>	↑ ↓ ↑ ↓ ↑		1.73
lanthanide metal ion	<sup>63</sup> Eu <sup>3+</sup>		↑ ↓ ↑ ↑ ↑ ↑ ↑	3.4
	<sup>64</sup> Gd <sup>3+</sup>		↑ ↑ ↑ ↑ ↑ ↑ ↑	7.94
	<sup>66</sup> Dy <sup>3+</sup>		↑ ↓ ↑ ↓ ↑ ↑ ↑ ↑	10.65

### Benefits of T<sub>1</sub> contrast agents

- Improve the T<sub>1</sub> relaxation creating a positive imaging effect with a growing and better signal, allowing getting an anatomic imaging with high spatial resolution.
- The bright signal stands out clearly from other pathological or biological conditions.

The first type of T<sub>1</sub> contrast agents was based on nanostructured platforms (such as silica, dendrimers, emulsions, and nanotubes) which have many anchoring sites for paramagnetic ions.<sup>[15]</sup> Such particles may contain a large number of paramagnetic payloads and produce strong T<sub>1</sub> contrast. On this matter, Lin and coworkers have synthesized silica nanoparticles and mesoporous silica containing a large number of Gd<sup>3+</sup> ions and developing multifunctional properties. Also, carbon nanotubes may serve as a framework that holds Gd<sup>3+</sup> ions, both on the surface or in their structural defects.<sup>[16, 17]</sup> In these materials, many metal ions are concentrated in a well-defined volume and their biological behavior and relaxivity are different than the complexing agents. In practice, this type of contrast agent is an extension of the paramagnetic complexes agents as the maximum number of ions is limited by the density of anchor groups on the surface. Also, their synthesis is very complicated and expensive, but the most significant limitation is their large overall size (> 100 nm), which is much larger than that of inorganic nanoparticles. To prevent their easy excretion by the RES and to compete with the small size of the T<sub>2</sub> contrast agents, their overall size must be <100 nm, which is satisfied by inorganic nanoparticles.<sup>[15]</sup>

Very recently, paramagnetic inorganic nanoparticles have been developed as new T<sub>1</sub> contrast agents. In order to be an effective T<sub>1</sub> contrast agent, the ratio between the transverse and longitudinal relaxivity (expressed as r<sub>2</sub>/r<sub>1</sub>), which is a parameter that allows to define a contrast agent as positive or negative, must be close to 1.

That is, nanoparticles should have large paramagnetic properties ( $r_1$ ) with negligible magnetic anisotropy (small  $r_2$ ).<sup>[2]</sup> For that reason, nanoparticles formed from some transition compounds are excellent candidates as  $T_1$  contrast agents since their surface contain a large amount of metal ions with a high magnetic moment.

### 2.4.1 Gadolinium based contrast agents

The most used  $T_1$  contrast agents are those based on Gadolinium, already widely used in clinical studies. Gadolinium oxide ( $Gd_2O_3$ ), gadolinium fluoride ( $GdF_3$ ), and gadolinium phosphate ( $GdPO_4$ ) nanoparticles showed an improvement in the contrast enhancement in  $T_1$ -weighted images with low  $r_2/r_1$  ratio. The physical properties and relaxivity of some  $T_1$  contrast agents based on inorganic nanoparticles are summarized in Tables 2.5 and 2.6. Usually, contrast agents based on  $Gd_2O_3$  nanoparticles are composed of a small core of  $<5$  nm and stabilized with shells of dextran, PEG, and silica.<sup>[18, 19]</sup> For example, water dispersible  $GdF_3$  nanoparticles (or  $GdF_3/LaF_3$ ) have been prepared with both positive surface charge, by conjugation with 2-aminoethyl phosphate groups ( $GdF_3/LaF_3$ : AEP), and negative surface charge, by coating with citrate groups ( $GdF_3$ : cit).<sup>[20]</sup>

**Table 2.5:** Properties  $T_1$  contrast agents based on inorganic nanoparticles. <sup>[2]</sup>

Name	Core Material	Surface	Diameter of Core [nm]	Hydrodynamic Diameter [nm]
Dextran-SPGO	$Gd_2O_3$	Dextran		26
PEG- $Gd_2O_3$	$Gd_2O_3$	PEG	3	
GadoSiPEG	$Gd_2O_3$	Polysiloxane-PEG	2.2	3.3
			3.8	5.2
			4.6	8.9
$GdF_3$ :cit	$GdF_3$	Citric acid		129.3
$GdF_3/LaF_3$ :AEP	$GdF_3/LaF_3$	2-Aminoethyl Phosphate		51.5
PGP/dextran-K01	$GdPO_4$	Dextran		23.2
MnO	MnO	PEG	7	
			15	
			20	
			25	
$FeCo/GC$	$FeCo$	Graphitic Carbon-PEG	4	30
			7	

### Gadolinium toxicity

Free gadolinium ( $Gd^{3+}$ ) is considered toxic because it tends to precipitate and to deposit in liver, lymph nodes and bones due to its absence in the normal metabolic pathways.

It can also obstruct the transport of calcium ions through the muscle cells, blocking the calcium flow into the cells of the nervous tissue, causing arrest of neuromuscular transmission. For these reasons, the conventional  $T_1$  contrast agents are presented as ionic complexes with chelating ligands which make them thermodynamically and kinetically stable and less toxic. Furthermore, it is important to take in consideration the trans-metallization process in which Gd can replace some metals such as Zn. This effect can be controlled by the stability of the complex: more stable chelate complexes, less likely to release Gd ions.<sup>[18]</sup>

**Table 2.6:** Relaxivity properties of contrast agents based on inorganic nanoparticles.<sup>[2]</sup>

Name	Core Material	Diameter of core [nm]	Relaxivity based on concentration of whole atoms		Relaxivity based on number of particles		Relaxivity based on surface		$B_0$ (T)
			$r_1$ [ $\text{mM}^{-1} \text{s}^{-1}$ ]	$r_2$ [ $\text{mM}^{-1} \text{s}^{-1}$ ]	$r_1$ [ $\text{mM}^{-1} \text{s}^{-1}$ ]	$r_2$ [ $\text{mM}^{-1} \text{s}^{-1}$ ]	$r_1$	$r_2$	
Gd-DTPA	Gd	ion	4.1	4.9	4.1	4.9			7
Dextran-SPGO	$\text{Gd}_2\text{O}_3$		4.8	16.9					7
PEG- $\text{Gd}_2\text{O}_3$	$\text{Gd}_2\text{O}_3$	3	9.4	13.4					1.5
GadoSiPEG	$\text{Gd}_2\text{O}_3$	2.2	8.8	11.4	3700	4800			7
		3.8	8.8	28.8	18600	60700			
		4.6	4.4	28.9	38800	65000			
PGP/dextran-K01	$\text{GdPO}_4$		13.9	15					0.47
GdF <sub>3</sub> :cit	$\text{GdF}_3$		3.17		$2.0 \times 10^7$		227.3[a]		14.2
GdF <sub>3</sub> /LaF <sub>3</sub> :AEP	$\text{GdF}_3/\text{LaF}_3$		2.71		$8.8 \times 10^5$		77.2[a]		14.2
PGP/dextran-K01	$\text{GdPO}_4$		13.9	15					0.47
MnO	MnO	7	0.37	1.74	3000	14000	33[b]	154[b]	3
		15	0.18	0.57	15000	46000	34[b]	121[b]	
		20	0.13	0.52	25000	99000	33[b]	102[b]	
		25	0.12	0.44	46000	165000	39[b]	139[b]	
FeCo/GC	FeCo	4	31	185					1.5
		7	70	644					

[a] Relaxivities based on the  $\text{Gd}^{3+}$  on the shell (unit:  $\text{mM}^{-1} \text{s}^{-1}$ ). [b] Relaxivities based on the surface area of nanoparticles (unit:  $\text{m s}^{-1}$ )

Headache, nausea, taste disturbance and skin rash are the most common side effects. Moreover anaphylactic reactions leading to death involving the respiratory and cardiovascular systems have been observed on 1/500,000 cases. Some studies have also shown that using gadolinium based contrast agents in patients suffering from kidney failure, increases the risk of nephrogenic systemic fibrosis (NSF). For those reasons, the FDA recommends avoiding these substances until there are no other viable alternatives.<sup>[18]</sup>

#### 2.4.2 New contrast agents based on Manganese

Some metal ions such as Mn (II), Fe (III) and Cu (II), despite having a smaller number of unpaired electrons and a lower magnetic moment, may offer an alternative to Gadolinium as  $T_1$  contrast agent.

In particular, Mn (II) ions play important roles in biological processes such as enzymes cofactors and the controlled release of neurotransmitters. Although there are some contrast agents based on manganese (II) complexes,  $Mn^{2+}$  itself in the form  $MnCl_2$  solution has been the most widely used, showing a contrast effect that reveals detailed physiological and biological information establishing a new category imaging, known as Manganese-enhanced MRI (MEMRI). In particular, MEMRI have been used for visualizing the anatomical structure of the brain as well as the neuronal activity which usually cannot be obtained by any other Gadolinium (II) based contrast agent.<sup>[7]</sup> Starting from the thermal decomposition of a Mn-oleate complex, it is possible to synthesize MnO nanoparticles dispersed in non-polar organic solvent whose particle size is controlled by varying both the solvent and the reaction time.

Hyeon et al have reported the encapsulation of MnO nanoparticles in a shell of poly Ethylene glycol (PEG) to make them biocompatible.<sup>[7]</sup> Figure 2.13.a) shows transmission electron microscopy (TEM) images of uniform, highly crystalline and water stable MnO nanoparticles with different sizes.<sup>[21]</sup> Moreover, as shown in Figure 2.13.b), nanoparticles with dimensions ranging from 7 to 25 nm showed a signal increase at the same concentration (5 mM), with brighter  $T_1$ -weighted images, thus confirming their potential applications as  $T_1$  contrast agents. The smaller the nanoparticle size, the brighter the signal in  $T_1$ -weighted images, which indicates that the shortening effect of  $T_1$  increases with the decrease of the nanoparticles size (Table 2.7). In this case, as stated before, MnO nanoparticles produce a decrease in both the longitudinal ( $T_1$ ) and transverse relaxation time ( $T_2$ ).

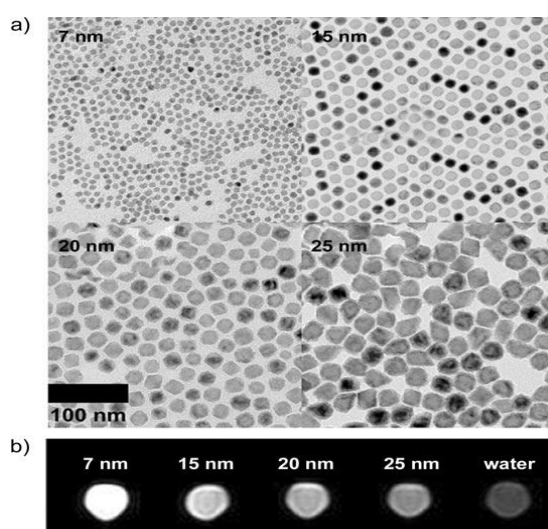


**Fig. 2.13:** a) TEM and b)  $T_1$ -weighted images of water dispersible MnO nanoparticles with different dimensions.  $T_1$ -weighted images were acquired under a 3T field.<sup>[7]</sup>

**Table 2.7:** Relaxivity properties of MnO nanoparticles with different size measured at 5mM.<sup>[7]</sup>

Nanoparticle size [nm]	Longitudinal relaxation				Transversal relaxation			
	$T_1^{[a]}$ [ms]	$r_1$ [ $\text{mM}^{-1} \text{s}^{-1}$ ]	$r_{1(N)}$ [ $\mu\text{M}^{-1} \text{s}^{-1}$ ]	$r_{1(S)}$ [ $\text{mS}^{-1}$ ]	$T_2^{[a]}$ [ms]	$r_2$ [ $\text{mM}^{-1} \text{s}^{-1}$ ]	$r_{2(N)}$ [ $\mu\text{M}^{-1} \text{s}^{-1}$ ]	$r_{2(S)}$ [ $\text{mS}^{-1}$ ]
7	481	0.37	3	33	85	1.74	14	154
15	624	0.18	15	34	95	0.57	46	121
20	707	0.13	25	33	120	0.52	99	102
25	752	0.12	46	39	132	0.44	165	139

The effectiveness of MnO nanoparticles as  $T_1$  contrast agents has been assessed by Hyeon et al. in mice treated with nanoparticles with a core of 25 nm.  $T_1$ -weighted images indicated as MONE-MRI (manganese oxide nanoparticle contrast-enhanced  $T_1$ -weighted MRI) showed an increased contrast in brain regions following by an accumulation of MnO nanoparticles in the tissue as demonstrated by the TEM images of the cortex obtained 72 h after injection (Fig. 2.14).

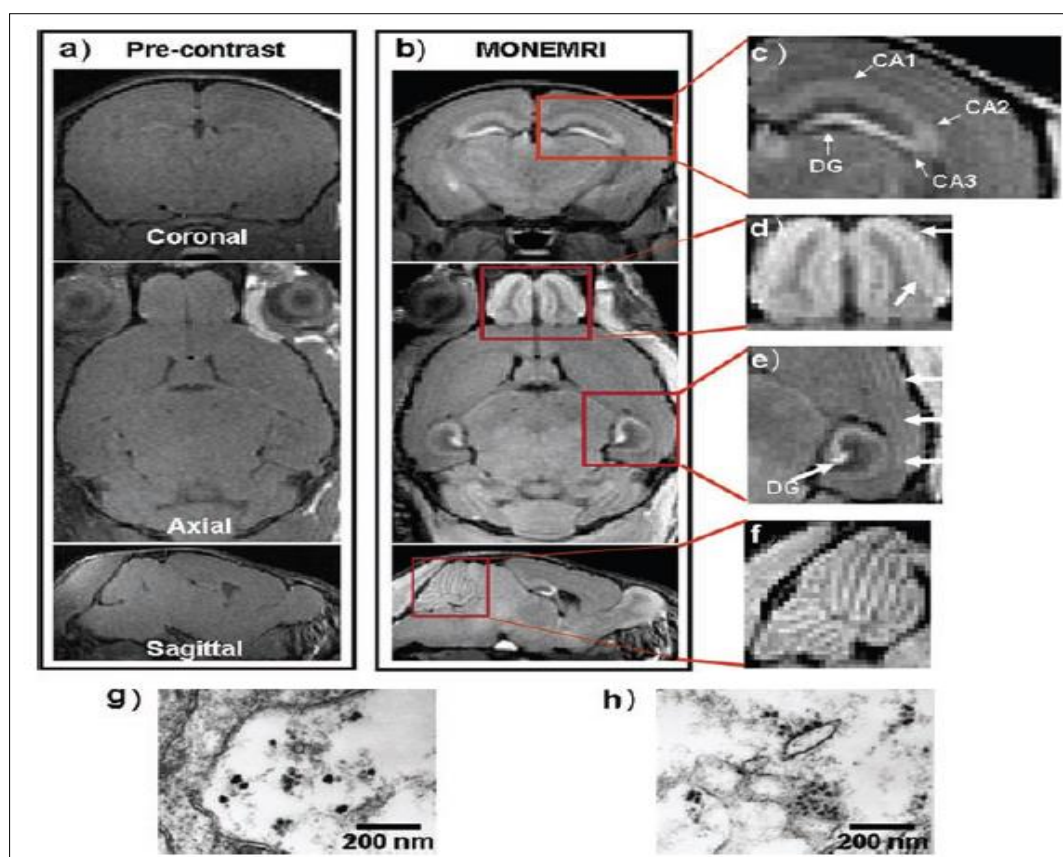


**Fig. 2.14:** a, b) coronal (top), axial (center), and sagittal views (bottom) of 3D  $T_1$ -weighted images before (a) and after (b) the administration of MnO nanoparticles. Images in (b) show a brighter contrast in brain structures due to the MnO nanoparticles accumulation. c) The hippocampus structure is revealed showing the *Cornu Ammonis* regions CA1, CA2, CA3, and the dentate gyrus (DG). d) Axial view showing the olfactory bulb. e) The head of the DG is clearly stated, and the cortical layers are visible. f) The structure of the cerebellum is clearly visible. Images g-h), TEM images of the cortex (g) and hippocampus (h) tissues showing the presence of MnO nanoparticles.<sup>[21]</sup>



The images of various brain structures suggest the potential applicability not only in basic research on neuroscience, but also to neurodegenerative disorders such as Parkinson's disease, Alzheimer, epilepsy and cortical dysplasia.

For the selective imaging of specific biomarkers in brain pathologies, MnO nanoparticles can be functionalized by conjugation with Her2 antibody for a selective target towards the epidermal growth factor receptors (EGFRs) which are overexpressed on the surface of brain cancer cells. Recent studies have reported the first biocompatible and nanostructured T<sub>1</sub> contrast agent for MRI applicable to different organs and body tissues, allowing obtaining clear T<sub>1</sub>-weighted images of the brain, liver, kidney and bone marrow from 5 days to 3 weeks after administration of MnO nanoparticles. Their distribution, accumulation in organs and tissues of interest as well as a tolerable low cellular toxicity open a new pathway for the development of contrast agents for molecular therapy and cellular imaging in medicine of the future.<sup>[22]</sup>

### **2.5. Application of MnO NPs for early diagnosis of Inflammatory Bowel Disease (IBD)**

The natural history of Crohn's disease involves the inflammation of the transmural intestine which often leads to narrowing of the lumen causing bowel obstruction. Histologically, a mixture of inflammatory and mesenchymal cells is presented together with components of the extracellular matrix with different degrees of fibrosis. Inflammatory intestinal stenosis often responds quickly to treatment with high doses of steroids as well as to therapy with powerful anti-tumor activity. This could help to relieve the intestinal obstruction, but it exposes the patient to many side effects such as the deleterious effects of steroids on the growth and development of children. Moreover, intestinal stenosis which is mostly of fibrotic nature, will not respond to these medical treatments, but it will require surgical resection.<sup>[23]</sup>

Currently, there are not clinical imaging modalities that enable physician to specifically determine the level of fibrosis present in intestinal stenosis. In this regard, J. Adler and collaborators have studied the magnetization transfer in magnetic resonance (MTMR) to face the need for a non-invasive technique for quantification of intestinal fibrosis in a mouse model with Crohn's disease.<sup>[24]</sup> MTMR describes images with different molecular properties compared to conventional MR. While the contrast between different tissues in MR is a function of the tissue properties and the parameters of the pulse sequence, MT generates contrast based on the fraction of immobilized macromolecules or phospholipids in the cell membrane of the tissues.

Because of its increased specificity, MT is more sensitive to changes in the collagen content which occur in intestinal fibrosis with tissue stenosis and, therefore, it is able to differentiate intestinal tissues containing less collagen (for example, inflamed tissues). In a study carried out by Adler et al, it was established that MT could help differentiate fibrotic from non-fibrotic tissue and that MT ratio would be correlated with the content of intestinal collagen in a well characterized rat model of Crohn's disease in both early and late stage of intestinal inflammation.<sup>[24]</sup> After injection, in an early stage, rats injected with PG-PS (purified peptidoglycan-polysaccharide) have developed inflammation while control animals were injected with human serum albumin (HSA). In the late stage, which begins about 14 days after the laparotomy, it was possible to identify intense inflammation and fibrosis. Furthermore, 21 days after the laparotomy, the rats develop thickening of the intestinal wall and intra abdominal adhesions.<sup>[24]</sup> After evaluation, the average MT ratio of 18 rats injected with PG-PS at the late stage (MT = 24.7 +/- 1.9) was significantly higher compared to the control rats (MT = 10.8 +/- 1.7). Furthermore, rats injected with PG-PS developed muscular hyperplasia and fibrotic thickness of the intestine, which was histologically seen as bands of collagen through the submucosa. On the other hand, the intestine of control animals showed up essentially normal, without fibrosis. MTMR images of rats with PG-PS, who developed intestinal fibrosis, have shown a thickened wall with intense red signal, representing a higher ratio on MT images while in the control rats this phenomenon did not occur. Therefore, it is possible to conclude that MT can help to identify intestinal fibrosis *in vivo* in a murine model of Crohn's disease. In addition, the MT ratio of fibrotic segments of the intestinal wall in rats with fibrosis induced by PG-PS compared to the non fibrotic intestine in control animals.<sup>[24]</sup>

MTMR is the first non-invasive imaging technique that can help to recognize intestinal fibrosis in a semiquantitative manner. Other imaging modalities have been investigated in an attempt to identify a non-invasive technique for the quantification of the intestinal fibrotic wall. Computed tomography (CT), although designed to detect fibrosis including the thickening of the bowel wall, has shown no improvement on contrast. Also, it has been seen that PET/CT is sensitive to inflammation but it is unable to describe differences between fibrosis, muscle hypertrophy and inflammation while MR enterography provides detailed images of the intestine and extraintestinal structures as well as other information clinically useful.<sup>[25]</sup>

MT imaging has the potential to be readily available for implementation in clinical practice since it uses a sequence pulse available on many RM units currently in use. The implementation of this sequence does not require hardware upgrades, but just some software programming. Some MT imaging tests are currently being conducted in humans to its assessment, to determine its resolution, and to demonstrate its reliability and accuracy in patients with Crohn's disease. If MT shows sensitivity for detection of fibrosis in human intestinal wall, it could directly help patient care.<sup>[24]</sup> Having the ability to quantify intestine fibrosis could help to determine whether a patient with obstructive symptoms has fibrotic stenosis requiring surgery or dilation; or if he or she has an inflammatory stenosis that is more likely to respond to medical diagnosis. Finally, this non-invasive method for determining the fibrotic content of small intestine stenosis in Crohn's disease may be used to direct experts into treatment decisions.<sup>[24]</sup>

## REFERENCES

1. Hashemi, R.H., W.G. Bradley, and C.J. Lisanti, *MRI: the basics*. Drug development and industrial pharmacy. 2012: Lippincott Williams & Wilkins.
2. Na, H.B., I.C. Song, and T. Hyeon, *Inorganic nanoparticles for MRI contrast agents*. *Advanced Materials*, 2009. **21**(21): p. 2133-2148.
3. Bellin, M.-F., *MR contrast agents, the old and the new*. *European journal of radiology*, 2006. **60**(3): p. 314-323.
4. Bulte, J.W. and M. Modo, *Nanoparticles in biomedical imaging: emerging technologies and applications*. Vol. 3. 2007: Springer Science & Business Media.
5. Xu, H., et al., *Preparation and preliminary evaluation of a biotin-targeted, lectin-targeted dendrimer-based probe for dual-modality magnetic resonance and fluorescence imaging*. *Bioconjugate chemistry*, 2007. **18**(5): p. 1474-1482.
6. Jun, Y.-w., et al., *Nanoscale size effect of magnetic nanocrystals and their utilization for cancer diagnosis via magnetic resonance imaging*. *Journal of the American Chemical Society*, 2005. **127**(16): p. 5732-5733.
7. Na, H.B., et al., *Development of a T1 contrast agent for magnetic resonance imaging using MnO nanoparticles*. *Angewandte Chemie*, 2007. **119**(28): p. 5493-5497.
8. Yoon, T.J., et al., *Specific targeting, cell sorting, and bioimaging with smart magnetic silica core-shell nanomaterials*. *Small*, 2006. **2**(2): p. 209-215.
9. Dubertret, B., et al., *In vivo imaging of quantum dots encapsulated in phospholipid micelles*. *Science*, 2002. **298**(5599): p. 1759-1762.
10. Wang, Y., et al., *"Pulling" nanoparticles into water: phase transfer of oleic acid stabilized monodisperse nanoparticles into aqueous solutions of  $\alpha$ -cyclodextrin*. *Nano Letters*, 2003. **3**(11): p. 1555-1559.
11. Tromsdorf, U.I., et al., *Size and surface effects on the MRI relaxivity of manganese ferrite nanoparticle contrast agents*. *Nano letters*, 2007. **7**(8): p. 2422-2427.
12. Harisinghani, M.G., et al., *Noninvasive detection of clinically occult lymph-node metastases in prostate cancer*. *New England Journal of Medicine*, 2003. **348**(25): p. 2491-2499.
13. Josephson, L., et al., *High-efficiency intracellular magnetic labeling with novel superparamagnetic-Tat peptide conjugates*. *Bioconjugate chemistry*, 1999. **10**(2): p. 186-191.
14. Lee, J.-H., et al., *Artificially engineered magnetic nanoparticles for ultra-sensitive molecular imaging*. *Nature medicine*, 2007. **13**(1): p. 95-99.
15. Flacke, S., et al., *Novel MRI contrast agent for molecular imaging of fibrin implications for detecting vulnerable plaques*. *Circulation*, 2001. **104**(11): p. 1280-1285.
16. Rieter, W.J., et al., *Nanoscale metal-organic frameworks as potential multimodal contrast enhancing agents*. *Journal of the American Chemical Society*, 2006. **128**(28): p. 9024-9025.

17. Sitharaman, B., et al., *Superparamagnetic gadonanotubes are high-performance MRI contrast agents*. Chem. Commun., 2005(31): p. 3915-3917.
18. McDonald, M.A. and K.L. Watkin, *Investigations into the physicochemical properties of dextran small particulate gadolinium oxide nanoparticles*. Academic radiology, 2006. **13**(4): p. 421-427.
19. Evanics, F., et al., *Water-soluble GdF3 and GdF3/LaF3 nanoparticles physical characterization and NMR relaxation properties*. Chemistry of materials, 2006. **18**(10): p. 2499-2505.
20. Hifumi, H., et al., *Gadolinium-based hybrid nanoparticles as a positive MR contrast agent*. Journal of the American Chemical Society, 2006. **128**(47): p. 15090-15091.
21. Lee, J.H., et al., *Manganese-enhanced magnetic resonance imaging of mouse brain after systemic administration of MnCl2: Dose-dependent and temporal evolution of T1 contrast*. Magnetic Resonance in Medicine, 2005. **53**(3): p. 640-648.
22. Shin, J., et al., *Hollow manganese oxide nanoparticles as multifunctional agents for magnetic resonance imaging and drug delivery*. Angewandte Chemie International Edition, 2009. **48**(2): p. 321-324.
23. Yaffe, B.H. and B.I. Korelitz, *Prognosis for nonoperative management of small-bowel obstruction in Crohn's disease*. Journal of clinical gastroenterology, 1983. **5**(3): p. 211-216.
24. Adler, J., et al., *Magnetization transfer helps detect intestinal fibrosis in an animal model of Crohn disease*. Radiology, 2011. **259**(1): p. 127-135.
25. Messaris, E., et al., *Role of magnetic resonance enterography in the management of Crohn disease*. Archives of Surgery, 2010. **145**(5): p. 471-475.



# Second section

## CONTENT

<b>Chapter III. MnO nanoparticles as contrast agents for MRI</b>	58
3.1. Materials	58
3.2. Experimental procedure	58
3.2.1. Synthesis of MnO nanoparticles	58
3.2.2. Nanoparticles characterization	60
3.2.3. Cellular viability and cytotoxic assays <i>in vitro</i>	61
3.2.4. MRI analysis <i>in vitro</i> and <i>in vivo</i>	62
3.2.5. Epifluorescence assays <i>ex vivo</i>	62
3.3. Results	63
3.3.1. Synthesis and characterization of MnO nanoparticles	63
3.3.2. MRI analysis <i>in vitro</i>	64
3.3.3. Biocompatibility Analysis	65
3.3.4. <i>In vivo</i> MRI analysis	67
3.3.5. Epifluorescence assay	68
3.4. Conclusions	70
<b>Chapter IV. Assessment of Gd-Fe<sub>3</sub>O<sub>4</sub> nanoparticles as a dual mode probe for diagnosis and treatment of cancer cells</b>	72



# Chapter III

## CHAPTER III

## MnO NANOPARTICLES AS CONTRAST AGENTS FOR MRI

**3.1. Materials**

Manganese Chloride tetrahydrate ( $\text{MnCl}_2 \cdot 4\text{H}_2\text{O}$ , 99%), Sodium Oleate (82%) and Oleic acid (analytical standard) acquired from Sigma Aldrich. Hexane (97%), Ethanol (99.8 %), Chloroform and Acetone (99%) acquired from PanReac AppliChem.

**3.2. Experimental procedure****3.2.1. Synthesis of MnO nanoparticles**

It was carried out the synthesis of MnO nanoparticles following a well established procedure described in literature consisting of two stages: overnight synthesis of the metal precursor from a Manganese salt and its further solvothermal decomposition (Fig 3.1).<sup>[1]</sup> By varying the reactions parameters such as solvent, temperature and reaction times it was possible to obtain nanoparticles with different size and morphology as reported in Table 3.1.

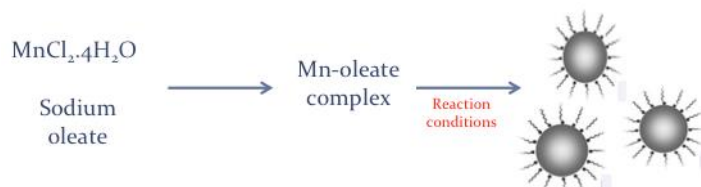


**Fig.3.1.** Schematic representation of the synthesis of MnO nanoparticles.

**Step 1: Synthesis of Mn-oleate complex**

0.792 mg of  $\text{MnCl}_2 \cdot 4\text{H}_2\text{O}$  (40 mmol) and 2.43 mg of sodium oleate (30 mmol) were dissolved in a mixture solution composed of 3 mL of ethanol, 7 mL of Hexane and 4 mL of distilled water. The resulting mixture was placed in a flask under vigorous magnetic stirring at 70 °C overnight. After completing the reaction, the solution was cooled down to room temperature and the stirring was stopped making evident the presence of two phases, an upper organic layer and an aqueous layer at the bottom. By using a separating funnel, it was possible to collect the organic phase which was washed several times with distilled water. Subsequently, the solution was dried by using a rotary evaporator allowing obtaining approximately 2 g of compound.

### Step 2: Solvothermal decomposition of Mn-oleate complex

2 g of Mn-oleate complex were dissolved in 14 mL of solvent (1-hexadecene or 1-octadecene) and then placed under magnetic stirring at 120 °C for 1 hour under argon flow. Following, the solution was heated till the reaction temperature (280 or 300 °C) during the time required (15, 30 or 60 min) according to the type of nanoparticle desired.

**Table.3.1.** Reaction conditions used for the synthesis of MnO nanoparticles.

Shape	Solvent	Temperature (° C)	Time (min)
Round	1-Hexadecene	280	60
Star-like	1- Hexadecene	280	30
Cubic	1-Octadecene	300	15

Once the reaction is completed, the solution was cooled down to room temperature, followed by three washings with acetone in centrifuge (8000 rpm, 6 minutes). After each wash, the supernatant was removed and the precipitated nanoparticles were re-dispersed in organic solvent (chloroform or hexane) by sonication.

### Nanoparticles coating and surface modification

Nanoparticles were coated with an amphiphilic polymer poly(Isobutylene-alt-maleic anhydride) (PMA) following a protocol similar to that described by Lin and coworkers (Fig. 3.2).<sup>[2]</sup> 0.04 mL of as-synthesized PMA (0.5 mM) were added to 0.5 mL of MnO nanoparticles dispersed in chloroform (2.78 mg/ml). By using a rotary evaporator, the solution was dried and further re-dispersed in 3 mL of sodium borate buffer (SBB) pH 12 by sonication. Subsequently, three washings with deionized water were carried out in a centrifuge (3200 rpm, 10 minutes) and the resulting MnO-PMA nanoparticles were collected. Similarly, it was possible to obtain fluorescent nanoparticles by encapsulating a fluorescent dye such as Fluorescein Isothiocyanate (Fitch) to the starting polymer (Fitch-PMA). Water-soluble MnO-PMA nanoparticles were modified by condensation with 2,20-(ethylenedioxy)bis(ethylamine) (EDBE) and further functionalized with N-succinimidyl-3-[2-pyridyldithio]-propionate (SPDP), following a procedure previously established in our laboratory.<sup>[3]</sup> The resulting thiol-reactive PDP functionalities were exploited for the conjugation of the molecular targeting (Fig. 3.3).

### Functionalization of MnO with anti-MAdCAM-1 (MnO-aMC1)

For their application in the diagnosis of IBD, it was required to conjugate the surface of MnO nanoparticles with anti-MAdCAM-1 (Mucosal Addressin Cell Adesion Molecule-1), a monoclonal antibody which is overexpressed in the colon to reduce T-cell mediated inflammation in some gastrointestinal diseases.

For the production of MnO-aMC1, anti-MAdCAM-1 was labeled with AF660 dye (Life Technologies) according to manufacturer's protocol and then dissolved in EDTA-PBS (1 mg/mL). Subsequently, it was added to the 2-mercaptoethanolamine kit (MEA, Thermo Scientific) and treated according to manufacturer's protocol to reduce the disulfide bridges between the two heavy chains of the IgG, obtaining the half-chain antibody portions. The half chains were immediately added to 1 mg of MnO nanoparticles (round only) and incubated at room temperature for 1 h. The remaining PDP functional groups were saturated with excess PEG<sub>500</sub>-SH which act as colloidal stabilizer and reduce nonspecific capture by the reticuloendothelial system. Excess chemicals and biological reagents were removed by dialysis, and MnO-aMC1 nanoparticles were collected.

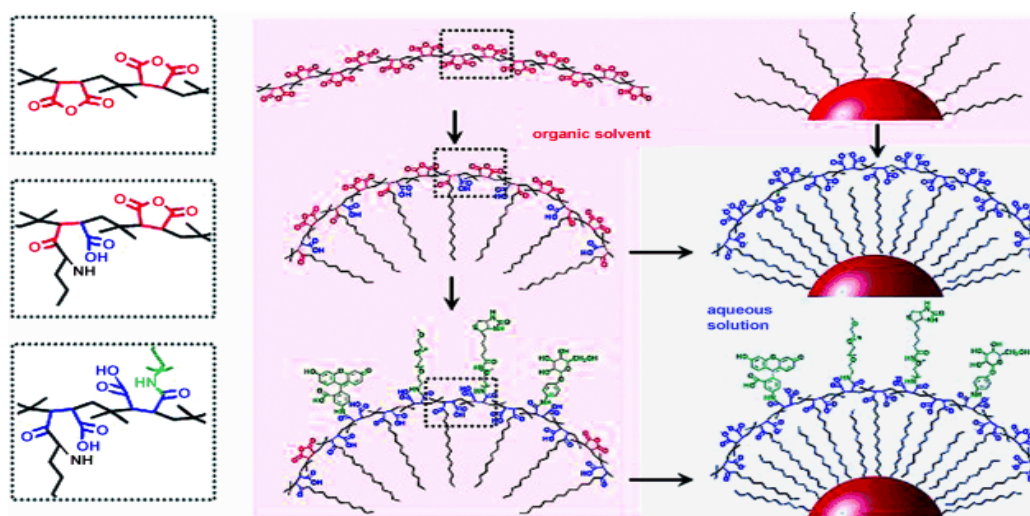
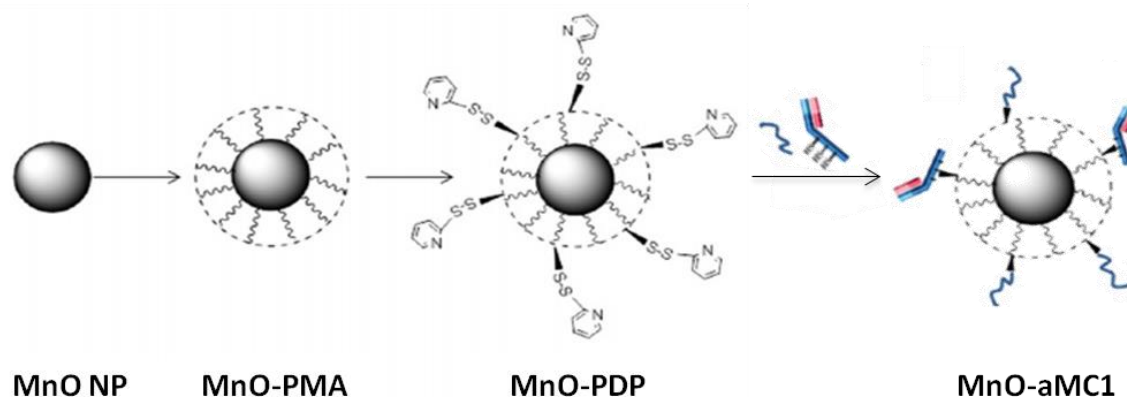


Fig.3.2. Schematic representation of the process for nanoparticles coating. <sup>[2]</sup>

#### 3.2.2. Nanoparticles characterization

The hydrodynamic diameter of the nanoparticles was determined by Dynamic Light Scattering (DLS) using a Malvern® 90 Plus DLS instrument operating with a 15 mW solid state laser. On the other hand, transmission electron microscope (TEM) images were obtained with a Zeiss EM-109 microscope operating at 80 k. In this case, the particles were diluted in Hexane (0.1mg/ml).



**Fig.3.3.** Step sequence for the preparation of MnO-aMC1 nanoparticles. <sup>[3]</sup>

Relaxivity properties were measured with a NMR Analyzer mq20 (BRUKER®) at 0.5 T. In this way, it was possible to determine the processes of decay of the magnetization of hydrogen nuclei (nuclear spins) after a radio frequency pulse. Appropriate RF pulse sequences were necessary to establish the different relaxation times and correlate them to the properties of synthesized materials. Finally, fluorescence of MnO nanoparticles was measured with a spectrofluorimeter Fluoromax-4 (HORIBA® Scientific). In this way, it was possible to analyze the fluorescence radiation emitted by the sample species allowing producing a spectrum as output by selecting an appropriate wavelength. To allow visualization of our samples, it was taken in consideration the absorption peak of FITC which is approximately 495 nm whereas the emission fluorescence is about 521 nm.

### 3.2.3. Cellular viability and cytotoxic assays *in vitro*

**MTT assay.** Murine endothelial cells SVEC4-10 were treated in Dulbecco's modified Eagle's medium (DMEM) containing 10% fetal bovine serum (FBS) at 37 °C for 24 hours. Three different types of MnO nanoparticles were placed on the plates at different concentrations (5, 20, 100 µg/ml) and incubated for 24, 48 and 72 hours. Cell viability quantification was performed by an optical absorbance reader (640/650 nm).

**Binding assay.** To allow interaction studies and cellular localization, MnO nanoparticles were conjugated with PEG-Fitch. The kinetics of interaction with the surface of SVEC4-10 cells was assessed by binding studies at 4 and 37 °C followed by the assessment of the percentage of cells bound to nanoparticles by flow cytometry. Subsequently, acquisition of images was possible by using fluorescence microscopy.

#### 3.2.4. MRI analysis *in vitro* and *in vivo*

For the acquisition of the MRI phantom *in vitro*, water-soluble MnO-PMA nanoparticles were prepared with concentrations of 0.001, 0.005, 0.01, 0.05, 0.2 mM of Mn ions in deionized water (based on Mn concentration measured by inductively coupled plasma atomic emission spectroscopy (ICP-AES)). The longitudinal ( $T_1$ ) and transverse ( $T_2$ ) relaxation times of the samples were measured at 25 °C using a 7 T Bruker MRI system.  $T_1$ -weighted images were obtained using an inversion-recovery fast spin-echo sequence (TR = 600 ms, TE = 10 ms).

In the other hand, to evaluate the contrast enhancement of the MnO NPs *in vivo*, it was developed a murine model of acute colitis induced by Dextran Sulfate Sodium (DSS) using C57BL mice of 6/8 weeks old (18-22 g). Animals were divided into four groups: group A, control animals (without any manipulation) and groups B, C and D treated with 3% DSS for 3, 5 and 7 days respectively in order to identify the earliest stage of onset of pathological symptoms. Experiments were conducted by assessing different parameters indicating disease activity and by *ex vivo* analysis of the colon of the treated animals in terms of histology, mRNA and proteins. Data obtained confirmed a rapid progression of the disease that starting from a mild phenotype at 3 days of treatment, it becomes very aggressive after 7 days of treatment. Acquired data allowed establishing the 5<sup>th</sup> day of treatment with DSS as the most convenient time for experiments with nanoparticles. Control animals were treated with a commercially available contrast agent (Gadovist) while mice of the remaining groups were injected with about 5 mg of three different MnO nanoparticles available (round, star like and cubic).

#### 3.2.5. Epifluorescence assays *ex vivo*

In order to assess the effectiveness of the MnO-aMC1 nanoparticles for targeting of IBD, AF660-labeled nanoparticles (85  $\mu$ g) were injected in the tail vein of mice with acute colitis induced by DSS after 5 days treatment. 4 and 24 hours after nanoparticles administration, mice were sacrificed and epifluorescence (Epf) imaging of dissected organs (colon and kidneys) was carried out in an IVIS Lumina II imaging system (Calipers Life Sciences). Images were acquired with a 720 nm emission filter, and excitation was scanned from 570 to 640 nm. All Epf values of the isolated tissues were normalized on the Epf obtained by IVIS acquisition of the nanoparticles solutions in a 96-well plate ( $\times 10^3$ ).

### 3.3. Results

#### 3.3.1. Synthesis and characterization of MnO nanoparticles

By varying the reactions parameters (solvent, temperature and time) it was possible to obtain highly monodisperse and crystalline MnO nanoparticles of three different morphologies: round, star-like and cubic as showed the TEM images (Figure.3.4).

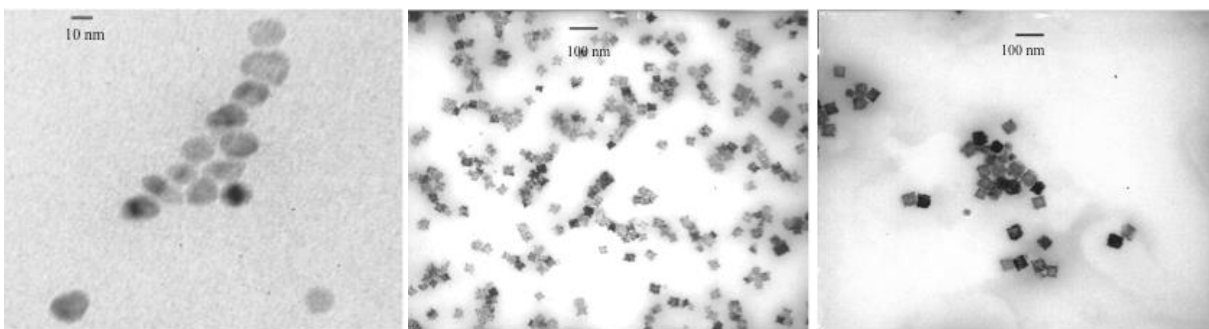


**Fig.3.4.** TEM images of MnO nanoparticles with different morphology: round (left) star-like (center) and cubic (right)

Measurements of their hydrodynamic diameter carried out by DLS, showed similar values to the data derived by analyzing the TEM images, with round nanoparticles of around 14 nm, while both cubic and star-like nanoparticles were found to be of around 40 nm size (Table 3.2).

To verify the storing and colloidal stability of the MnO nanoparticles after their transfer from the organic phase to the aqueous media, all three types of nanoparticles were dispersed in PBS at different pH and changes in size were measured by DLS through time. Results showed nanoparticles stability for more than 4 weeks. Only in extreme conditions (pH 4 and pH 12) nanoparticles exhibit an increase in the dimensions due to their aggregation (Fig. 3.5).

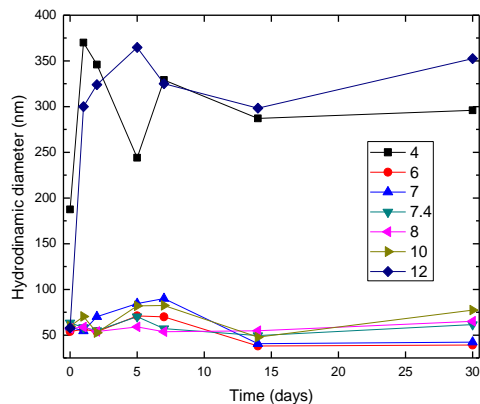


**Fig.3.5:** Hydrodynamic diameter of round MnO nanoparticles at different pH.

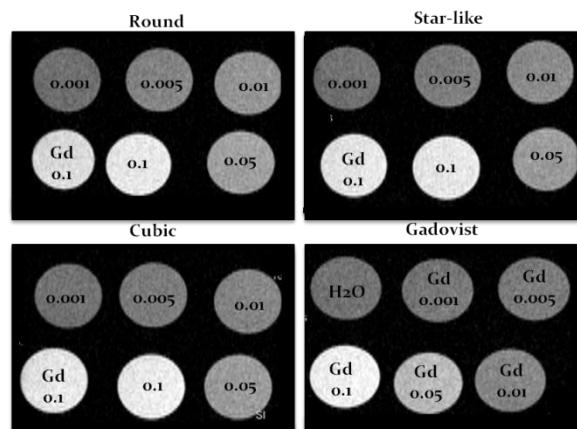
**Table 3.2.** Physical properties of MnO nanoparticles

Morphology	Hydrodinmic diameter (DLS)	Dimension (TEM)	$r_1$ ( $\text{mM}^{-1}\text{s}^{-1}$ )	$r_2$ ( $\text{mM}^{-1}\text{s}^{-1}$ )	$r_2/r_1$
Rotonde	$14,2 \pm 0,2$	$10 \pm 1$	3.09	4.91	1.59
Stellate	$36,1 \pm 0,3$	$30 \pm 1$	7.95	9.55	1.21
Cubiche	/	40x40	0.58	0.98	1.69

In order to determine the magnetic properties of the nanoparticles, samples were exposed to a magnetic field of 0.5 T. Measures of the longitudinal ( $T_1$ ) and transversal ( $T_2$ ) relaxation times at different concentrations of  $\text{Mn}^{2+}$  ions allowed to determine the relaxivity values  $r_1$  and  $r_2$  for all three types of nanoparticles (Table 3.2). Although results showed differences in relaxivity values for each kind of nanoparticles, the contrast enhancement on the  $T_1$ -weighted images did not show any significant difference between the three preparations (Fig 3.6). This can be explained since to assess the effectiveness of a positive contrast agent, it is necessary to take in consideration also the contribution of the transversal component of relaxivity ( $r_2$ ) via the ratio  $r_2/r_1$ . Indeed, the latter showed similar values for all three types of nanoparticles.

### 3.3.2. MRI analysis *in vitro*

$T_1$ -weighted images *in vitro* of MnO nanoparticles showed an increase in the contrast enhancement by increasing the concentration of  $\text{Mn}^{2+}$  ions similar for all three samples (Fig. 4.6), highlighting what has been explained in the previous section. These changes in intensity are comparable to those shown by the Gadovist®, a commercial contrast agent based on Gd currently in use in clinical practice. The bright signal enhancement showed in the  $T_1$ -weighted MRI manifests the potential applications of these nanoparticles as a  $T_1$  contrast agent.

**Fig.3.6:**  $T_1$ -weighted images of MnO nanoparticles with different morphology



### 3.3.3. Biocompatibility Analysis

MTT assay. From the results obtained, it was observed that exposure to 5 or 20  $\mu\text{g/mL}$  of nanoparticles for 24, 48 or 72 hours does not affect the proliferation of SVEC4-10 while high concentrations (100  $\mu\text{g/mL}$ ) seemed to be toxic to the cells (Fig.3.7).

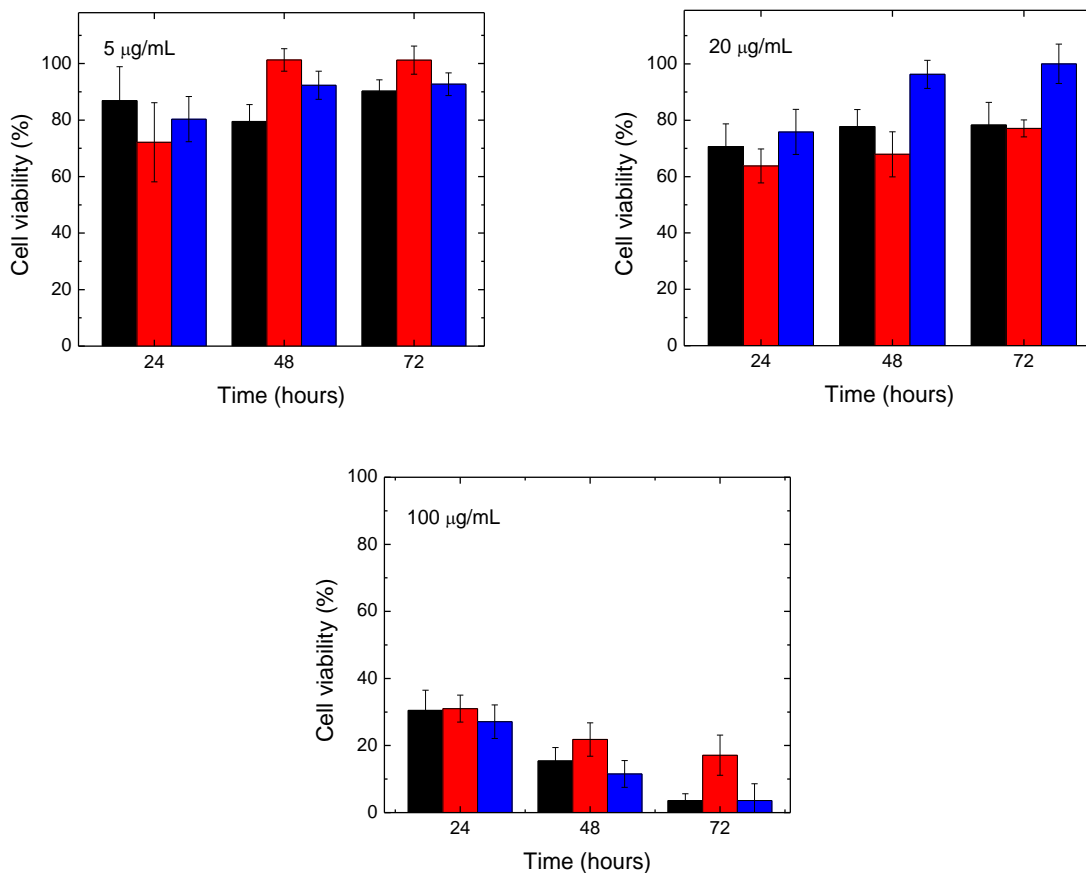


**Fig.3.7.** Cell viability at different NPs concentration for all three morphologies: cubic (black), star-like (red) and round (blue)

Binding assay. The kinetics of interaction with the surface of the cells was assessed by binding studies at 4 and 37  $^{\circ}\text{C}$  and further analysis of the percentage of cells bound to nanoparticles by flow cytometry. After incubation with 5 or 20  $\mu\text{g/mL}$  of nanoparticles, only a small percentage of cells were specifically bind nanoparticles (Fig. 3.8). Only values between 1 and 10% for nanoparticles round and star-like and up to a maximum of 20% for cubic nanoparticles were taken in consideration.

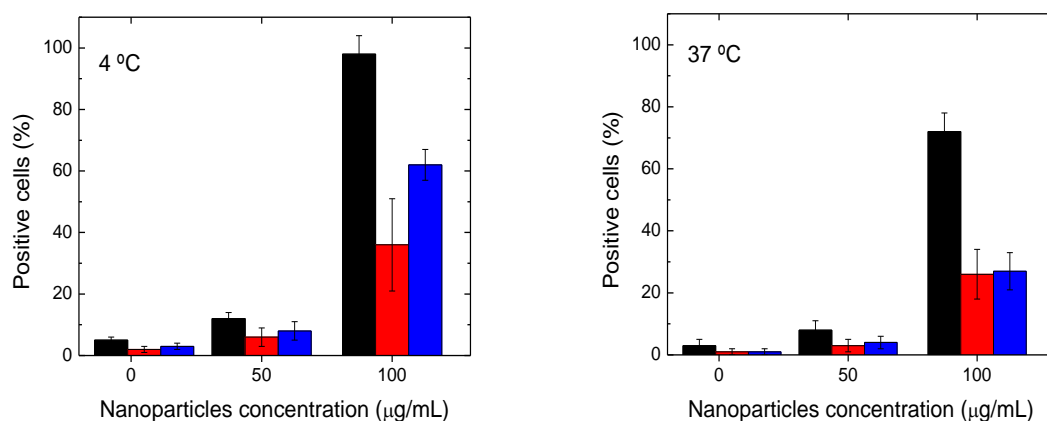


**Fig.3.8.** Binding assay at 4 and 37 ° C for three types of MnO NPs: cubic (black), star-like (red) and round (blue).

Successively, fluorescence microscopy allowed evaluating the internalization of MnO nanoparticles in cells. Images obtained showed that the nanocomposites were located in the cell membrane at the early stage, moving then to a cytoplasmic or diffused localization (probably by endocytic vesicles). In particular, cubic nanoparticles entered cells immediately after one hour of incubation, while round and star-like nanoparticles showed a delayed internalization.

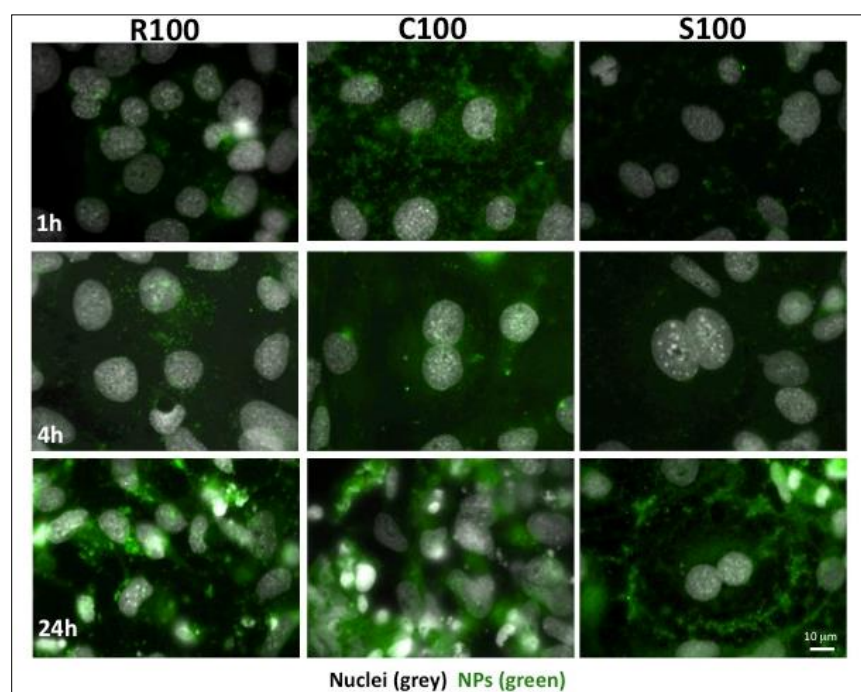


**Fig.3.9.** Fluorescence microscopy images of nanoparticles conjugated with PEG-FITC at 100 µg/mL measured after 1, 4 and 24 hours. Round (left), cubic (center) and star-like (right).

### 3.3.4. *In vivo* MRI analysis

As stated in the previous sections, since there were no significant differences in the behavior of all three type of nanoparticles tested (round, star-like and cubic), for practical purposes only round nanoparticles has been taken in consideration for further experiments *in vivo* (MRI and epifluorescence).

MRI images *in vivo* were acquired in acute colitis-bearing mice before and at different times (20 min, 1 hour and 24 hours) after intravenous administration of MnO-PMA nanoparticles. Preliminary results showed that 20 minutes after injection there was an improvement in the contrast enhancement of the intestinal walls (yellow arrows, Fig.3.10), and also slightly in the liver and kidneys (red arrows, Fig.3.10). After 4 hours, there is an evident increase in the signal in the peritoneum as well as in liver and kidneys, while a decrement is showed in the intestinal walls compared to the acquisition at 20 minutes. Finally, 24 hours post inoculation the signal disappears from the intestinal wall and liver, but it still remains in the peritoneum, being more evident in kidneys and bladder which as evidence of active renal excretion.

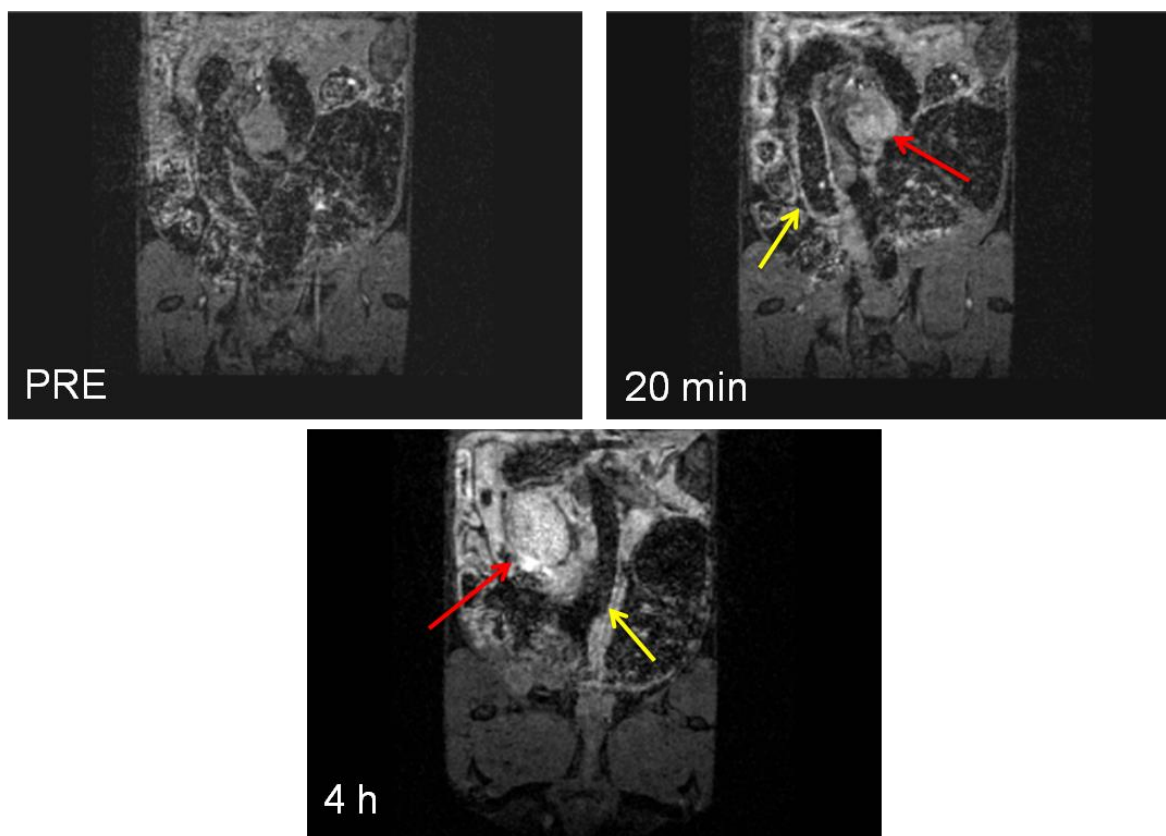


**Fig.3.10.** Magnetic resonance imaging of mice with induced colitis before inoculation (PRE) and after inoculation of MnO nanoparticles after 20 minutes and 4 hours.

Regarding the control mice inoculated with Gadovist<sup>®</sup>, the behavior found was very similar to that from the nanoparticles tested. 20 minutes after inoculation, it was shown an increase of the contrast enhancement in the walls of the colon. After four hours, very low signal was detected in the area affected by the disease and 24 hours after injection, signal enhancement was showed only on kidneys and bladder evidencing renal excretion. Finally, it was found a strong intravascular presence of the commercial contrast agent, indicating long blood circulation time compared to nanoparticles.

### 3.3.5. Epifluorescence assay

In order to evaluate the effectiveness of active molecular recognition in targeting Mad-CAM-1 cells, *ex vivo* Epifluorescence (Epf) images of the colon of acute colitis-bearing mice were acquired 24 hours after injection of nanoparticles (Figure.3.11). Results indicated that the MnO-aMC1 nanoconstruct was able to specifically target the region of interest (Fig.3.11.b) compared to the control sample MnO-IgG (Fig.3.11.a), showing a strong increase in fluorescence intensity in the affected area due to nanoparticles accumulation.

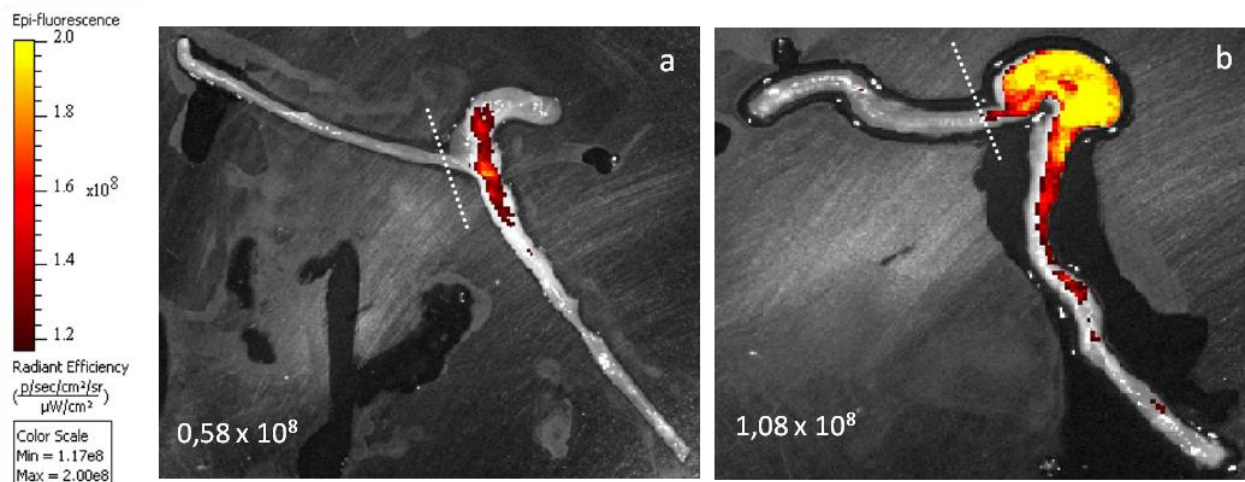


**Fig.3.11.** Epifluorescence images of the colon of acute colitis-bearing mice 24 hours after injection of MnO-IgG (a) and MnO-aMC1 nanoparticles (b).

As the injected solutions of MnO-IgG and MnO-aMC1 showed a significant difference in intrinsic fluorescence intensity, it was necessary to normalize the recorded Epf values on the fluorescence intensity of injected solution, in order to provide a more appropriate comparison between both nanocomplexes.

Preliminary results obtained confirmed a strong decrease over time of MnO-IgG Epf intensity in colon while MnO-aMC1 Epf showed an intensity increase over time evidencing the accumulation of this nanocomposite due to their anchorage to the inflammatory site which was mediated by the targeting of MAdCAM-1 cells overexpressed in the diseased tissue (Fig.3.12). In the other hand, regarding the kidneys, it was shown an increase on the MnO-IgG Epf after 24 hours indicating renal excretion. At the same time, MnO-aMC1 Epf intensity seemed to be very low 4 hours after injection, becoming almost undetectable after 24 hours.

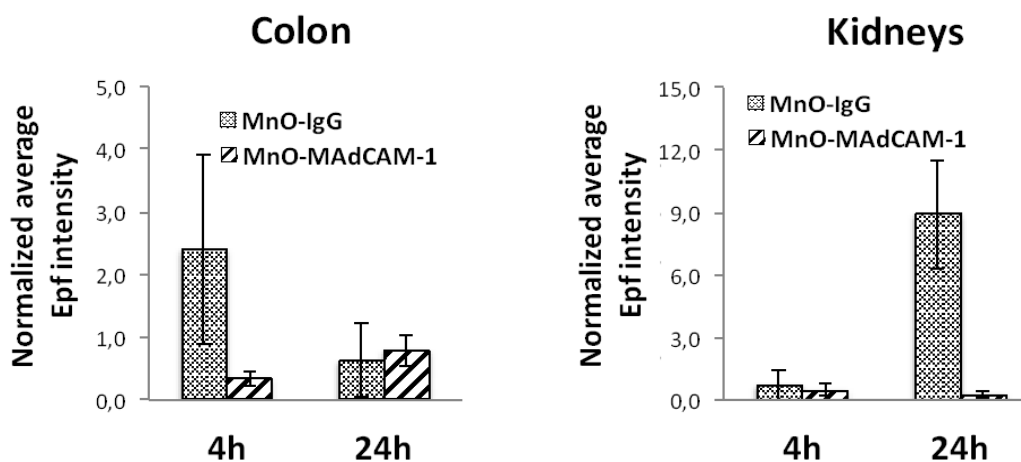


**Fig.3.12.** Averaged Epi fluorescence intensity of the colon and kidneys of acute colitis-bearing mice 4 and 24 hours after injection of nanocomposites.

### 3.4. Conclusions

Synthesized MnO nanoparticles with different morphologies showed optimal physical-chemical properties as well as colloidal stability through time. Their capacity of decrement the  $T_1$  relaxation time of water protons *in vitro* was similar for all three morphologies tested and analogous to the commercial contrast agent Gadovist®.

Cytotoxic assays of the different forms of MnO nanoparticles showed that exposure to 5 or 20  $\mu\text{g/mL}$  of nanoparticles for 24, 48 or 72 hours does not affect the proliferation of SVEC4-10. In addition, the nanoparticles concentrations tested do not alter the basal level of apoptosis in SVEC4-10 which was observed thanks to their conjugation with specific markers after 4 or 24 hours of incubation with the nanoparticles. At the same time, the nanocrystals saturated with polyethylene glycol (PEG) and marked with the fluorescent molecule FITC, allowed to assess their cellular localization by binding assays and cellular interaction studies by flow cytometry.

It was developed a mouse model of acute colitis induced by 5 days treatment with Dextran Sodium Sulfate (DSS) in drinking water using C57BL mice aging 6 to 8 weeks old (18-22 grams).  $T_1$ -weighted images acquired *in vivo*, showed a signal enhancement in the intestinal walls 20 min and 4 hours after nanoparticles injection, evidencing accumulation of MnO nanoparticles in the inflammatory site. Moreover, 24 after injection there was a signal increase in kidneys and bladder, indicating renal excretion. Results obtained were similar to those from Gadovist®.

Finally, MnO nanoparticles engineered with anti-MAdCAM-1 showed a strong increase in Epifluorescence intensity in the affected area compared with control MnO-IgG nanoparticles, confirming their accumulation in the inflammatory tissue.

In this way, we demonstrated the potential application of these MnO nanoparticles as a  $T_1$  contrast agent. Suggested experiments in the future include the assessment and establishment of the wash out time of the nanoparticles, as well as their biodistribution.

# Chapter IV

## CHAPTER IV

ASSESSMENT OF Gd-Fe<sub>3</sub>O<sub>4</sub> NANOPARTICLES AS A DUAL MODE PROBE  
FOR DIAGNOSIS AND TREATMENT OF CANCER CELLS

As part of the complementary formation in the MRI field, during my last year of doctorate school I took part of an attachment program for PhD students at the Magnetic Resonance Imaging Group at the Singapore Bioimaging Consortium (SBIC) which is part of the Agency for Science, Technology and Research (A\*STAR), headed by Dr. Kai-Hsiang Chuang.

During that period, it was carried out a project regarding the assessment of the magnetic properties of Gd doped Iron oxide nanoparticles (IONPs), and their efficacy as a dual mode tool for the diagnosis (MRI) and treatment (Hyperthermia) of cancer tumors (Fig.4.1). This work was conducted in collaboration with the Department of Materials Science and Engineering at the National University of Singapore (NUS), under the supervision of Prof. Ding Jung.

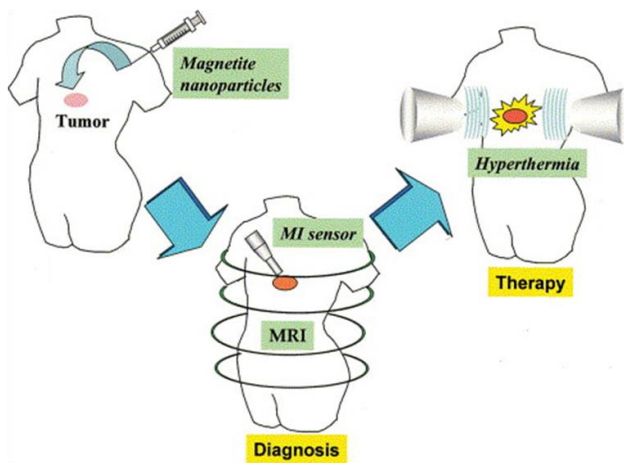


**Fig.4.1.** Schematic representation of a dual mode tool for diagnosis and treatment of cancer.

The importance of this work relies on the fact that nowadays one of the biggest challenges of modern medicine, so far not satisfactorily achieved, is cancer treatment. Besides the existing standard therapies based on surgery, chemotherapy, irradiation, or combinations of them, there are many alternative therapies among which hyperthermia have been used in clinical practice.<sup>[4]</sup>



Thermal energy is emerging as an important mean of triggering functions for various applications in biomedical systems. For example, gold nanoparticles can be successfully used to convert photons into thermal energy in drug release systems and for photothermal cancer therapy.<sup>[5,6]</sup> However, limited penetration depth and interferences of photons with tissues and surrounding media could hamper the effectiveness of these materials. Magnetic nanoparticles are also attracting considerable interest for their ability to mediate heat induction. When an external alternating current (AC) magnetic field is applied, a magnetization reversal process occurs and thermal energy is produced continuously as these particles return to their relaxed states. Because this magnetic heat induction makes use of radiofrequency electromagnetic waves, tissue penetration is not limited.<sup>[5]</sup> In addition to its non-invasive character, this thermal energy generation technique via magnetic nanoparticles mediators can be controlled remotely and actuated on-command.

In recent past, the combination of diagnosis and hyperthermia treatment of tumors has emerged as a potential research field where nanoparticles can target a tumor. These nanoparticles enhance the diagnosis and localization of specific tumor characteristics by multimodal imaging techniques including optical, magnetic resonance, positron emission tomography, computed tomography, and X-ray techniques.<sup>[7]</sup>

In local hyperthermia, the temperature increase with respect to standard body temperature is considered to be therapeutically useful over a relatively broad temperature range where different mechanisms of cell damaging occur with increasing temperature. Some of the most commonly used therapies include: treatments at temperatures of 42 - 45 °C for up to few hours combining other assisting agents (radiation or chemotherapy) for reliable killing of tumor cells. In contrast, thermoablation aims for the thermal damage of all tumor cells by applying temperatures in excess of at least 50 °C in the tumor region for exposure times of at least few minutes. Though these short treatment times and the resulting reliable tumor damage look advantageous, there are concerns considering critical systemic side effects such as shock syndrome due to sudden release of large amounts of necrotic tumor material and major inflammatory response.<sup>[8]</sup> In the following, both therapy modalities are comprised as magnetic particle hyperthermia (MPH). In any case, the amount of nanoparticles to be applied should be as small as possible in order to reach the therapy temperature with minimum particle concentration in tissue. For that reason, the specific heating power of the magnetic nanoparticles in magnetic AC fields should be as high as possible.

Successful application of MPH requires synthesis of stable colloidal suspensions of nanoparticles in biocompatible fluids (water or saline solution) that maintain their stability in biological media such as blood or plasma.<sup>[9-12]</sup> The particles must also produce a predictable and sufficient amount of heat, or specific absorption rate (SAR) measured in W/g, at modest particle concentrations (in order to limit toxicity) when exposed to AMF amplitudes that can be applied safely to large regions of tissue.<sup>[13]</sup> Thus, the surface chemistry, size, and magnetic properties of the particles must be engineered to meet demanding, even competing, performance criteria.<sup>[14]</sup>

Knowledge of the specific characteristics that are important for delivering the maximum heat dose per gram of injected material is essential for the successful design of a nanoconstruct for hyperthermia applications. The most influential characteristics include the saturation magnetization, anisotropy, relaxation time of the magnetic moments, amplitude and frequency of the external AMF, and intratumor particle concentration and distribution.<sup>[14]</sup> The distribution and amount of heat deposited to the tumor are related to each of these parameters and are integral to successful therapeutic outcome. However, some practical limitations due to physiologic constraints imposed by either tumor biology or toxicology, can affect the achievable value of each parameter.

Saturation magnetization is determined by choice of material and nanoparticle size, but few magnetic materials with large saturation moments (e.g., Co) are biocompatible. The choice of particle size is constrained by the physical and physiologic realities of the application. Field amplitude and frequency can be increased, but the power required to generate the field can become prohibitive, particularly at high frequency. Also, the non-specific coupling of the alternating magnetic field (AMF) energy with tissue becomes detrimental.<sup>[14]</sup>

There are four possible mechanisms for heat generation by magnetic materials when exposed to an AMF: (1) hysteresis, (2) Néel paramagnetic switching (relaxation), (3) friction from Brownian rotation (viscous suspensions) and (4) eddy current. Although contributions from all four mechanisms can lead to achieving the total heat generated by a particular magnetic sample, it is expected that only one or two of the mechanisms will dominate.<sup>[14]</sup> This is determined by the properties of the magnetic material and the magnetic field.

The heating capacity of magnetic nanoparticles results from the magnetic losses due to different processes of magnetization reversal which depends in different manners on the applied AC magnetic field amplitude and frequency.<sup>[14]</sup>

Moreover, there is a strong dependence of the structural properties of magnetic particle like size, width of size distribution, shape and crystallinity. For example, regarding their size, some researchers have shown that largest values (up to 1 kW/g) of SLP may be achieved in the transition range from superparamagnetic to stable ferromagnetic properties of the nanoparticles. However, the reason for the preference of very small magnetic nanoparticles is mainly due to the colloidal stability in the small particle range below about 10 nm.<sup>[13,14]</sup>

There is a multitude of known magnetic materials currently in use, however, for biomedical applications most of investigations have been focused on magnetic iron oxides Fe<sub>3</sub>O<sub>4</sub> (magnetite) and  $\gamma$ -Fe<sub>2</sub>O<sub>3</sub> (maghemite) which have been proved to be well tolerated by the human body.<sup>[7]</sup>

Recently, in an attempt to develop new nanoparticles with high thermal energy transfer capability, recently it have examined the effects of size and composition on the magnetic heating power of ferrite magnetic nanoparticles (MFe<sub>2</sub>O<sub>4</sub>, M = Mn, Fe, Co).<sup>[5]</sup> Considering that the SLPs of nanoparticles depend on nanoparticles size, composition and magnetic field, it was found that Fe<sub>3</sub>O<sub>4</sub> nanoparticles had SLPs values of 152, 349 and 333 W/g for diameters of 9, 12 and 15 nm, respectively. Similarly, MnFe<sub>2</sub>O<sub>4</sub> had a SLP maximum of 411 W/g at 15 nm and CoFe<sub>2</sub>O<sub>4</sub> had its SLP maximum of 443 W/g at 9 nm. Unfortunately, these values do not significantly exceed those reported for conventional magnetic nanoparticles, indicating that size and compositional effects are marginal.<sup>[2]</sup> For that reason, taking advantage of the exchange coupling between a magnetically hard core and a magnetically soft shell to tune the magnetic properties of the nanoparticles and maximize the specific loss power, which is a gauge of the conversion efficiency, it have been proposed the assessment of the Gd doped Fe<sub>3</sub>O<sub>4</sub> nanoparticles as a dual mode tool for the diagnosis (MRI) and treatment (Hyperthermia) of cancer tumors.

In order to achieve the aim of this study, MRI acquisitions *in vivo* and biodistribution studies were conducted in our facilities at SBIC on six week old female mice with U87MG xenograft tumor using a 7T Bruker® clinic scan following IACUC ethical policies regarding the use of animal for research purposes. At the same time, it is important to mention that the samples tested, were previously synthesized and well characterized at Prof. Ding's lab at NUS.

Preliminary results demonstrated considerable accumulation of Gd doped IONPS in the tumor after their administration. This could be due to the enhanced permeability and retention (EPR) effect which is a unique phenomenon of solid tumors related to their anatomical and pathophysiological differences from normal tissues.<sup>[12]</sup>

The high vascular density which is typical in solid tumors, together with large gaps existing between endothelial cells in tumor blood vessels, show selective extravasation and retention of macromolecules thus allowing to the development of anticancer therapy.

Due to the magnetic properties of the Gd doped  $\text{Fe}_3\text{O}_4$  nanoparticles tested; it was possible to quantify the deposited heat dose to the tumor. Correlating heat dose with tissue temperature rise and therapeutic outcome offers the tools clinicians require to develop and use prescriptive thermal treatment plans for their patients.<sup>[13]</sup> Deposition in tumor could bring to an increase in the local temperature and more localized heat deposition, providing hyperthermia treatment with nearly complete regression of tumors in mice.<sup>[14]</sup> In this way, the design of this nanoconstructs could be used as a dual probe, allowing both diagnosis and treatment of tumor in mice.

By the moment of writing these lines, and as a result of the work carried out by the team in both SBIC at NUS groups, a manuscript is being preparing for submission into a high impact factor journal. However, due to confidential character of the project, and taking in account intellectual property matters, it was not allowed to disclose any further detail and results regarding this work.

## REFERENCES

1. Na, Hyon Bin, et al. *Development of a T1 contrast agent for magnetic resonance imaging using MnO nanoparticles*. *Angewandte Chemie*, 2007. **119**(28): p. 5493-5497.
2. Lin, Cheng-An J., et al. *Design of an amphiphilic polymer for nanoparticle coating and functionalization*. *Small*, 2008. **4**(3): p. 334-341.
3. Fiandra, Luisa, et al. *Assessing the in vivo targeting efficiency of multifunctional nanoconstructs bearing antibody-derived ligands*. *ACS nano*, 2013. **7**(7): p. 6092-6102.
4. Falk, M. H., and R. D. Issels. *Hyperthermia in oncology*. *International Journal of Hyperthermia*, 2001. **17**(1): p. 1-18.
5. Lee, Jae-Hyun, et al. *Exchange-coupled magnetic nanoparticles for efficient heat induction*. *Nature nanotechnology*, 2011. **6**(7): p. 418-422.
6. Hergt, Rudolf, et al. *Magnetic particle hyperthermia: nanoparticle magnetism and materials development for cancer therapy*. *Journal of Physics: Condensed Matter*, 2006. **18**(38): p. S2919.
7. Moroz, P., S. K. Jones, and B. N. Gray. *Magnetically mediated hyperthermia: current status and future directions*. *International Journal of Hyperthermia*, 2002. **18**(4): p. 267-284.
8. Sharma, R., and C. J. Chen. *Newer nanoparticles in hyperthermia treatment and thermometry*. *Journal of Nanoparticle Research*, 2009. **11**(3): p. 671-689.
9. Adair, Eleanor R., and David R. Black. *Thermoregulatory responses to RF energy absorption*. *Bioelectromagnetics*, 2003. **24**(S6): p. S17-S38.
10. Owens, Donald E., and Nicholas A. Peppas. *Opsionization, biodistribution, and pharmacokinetics of polymeric nanoparticles*. *International journal of pharmaceutics*, 2006. **307**(1): p. 93-102.
11. Majewski, Peter, and Benjamin Thierry. *Functionalized magnetite nanoparticles—synthesis, properties, and bio-applications*. *Critical Reviews in Solid State and Materials Sciences*, 2007. **32**(3-4): p. 203-215.
12. Gupta, Ajay Kumar, et al. *Recent advances on surface engineering of magnetic iron oxide nanoparticles and their biomedical applications*. (2007): 23-39.
13. DeNardo, Sally J., et al. *Development of tumor targeting bioprobes (111In-chimeric L6 monoclonal antibody nanoparticles) for alternating magnetic field cancer therapy*. *Clinical Cancer Research*, 2005. **11**(19): p. 7087s-7092s.
14. Dennis, C. L., et al. *Nearly complete regression of tumors via collective behavior of magnetic nanoparticles in hyperthermia*. *Nanotechnology*. 2009. **20**(39): p. 395103.
15. Fang, Jun, Hideaki Nakamura, and Hiroshi Maeda. *The EPR effect: unique features of tumor blood vessels for drug delivery, factors involved, and limitations and augmentation of the effect*. *Advanced drug delivery reviews*, 2011. **63**(3): p. 136-151.
16. Dennis, C. L., et al. *Nearly complete regression of tumors via collective behavior of magnetic nanoparticles in hyperthermia*. *Nanotechnology*, 2009. **20**(39): p. 395103.

17. Lee, Jae-Hyun, et al. *Exchange-coupled magnetic nanoparticles for efficient heat induction*. Nature nanotechnology, 2011. **6**(7): p. 418-422.